NASA / TP-2000-210299

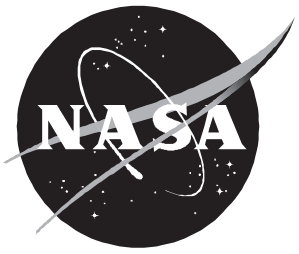

An Improved Elastic and Nonelastic Neutron Transport Algorithm for Space Radiation

Martha S. Clowdsley and John W. Wilson
Langley Research Center, Hampton, Virginia

John H. Heinbockel
Old Dominion University, Norfolk, Virginia

R. K. Tripathi, Robert C. Singleterry, Jr., and Judy L. Shinn
Langley Research Center, Hampton, Virginia

July 2000

The NASA STI Program Office . . . in Profile

Since its founding, NASA has been dedicated to the advancement of aeronautics and space science. The NASA Scientific and Technical Information (STI) Program Office plays a key part in helping NASA maintain this important role.

The NASA STI Program Office is operated by Langley Research Center, the lead center for NASA's scientific and technical information. The NASA STI Program Office provides access to the NASA STI Database, the largest collection of aeronautical and space science STI in the world. The Program Office is also NASA's institutional mechanism for disseminating the results of its research and development activities. These results are published by NASA in the NASA STI Report Series, which includes the following report types:

- TECHNICAL PUBLICATION. Reports of completed research or a major significant phase of research that present the results of NASA programs and include extensive data or theoretical analysis. Includes compilations of significant scientific and technical data and information deemed to be of continuing reference value. NASA counterpart of peer-reviewed formal professional papers, but having less stringent limitations on manuscript length and extent of graphic presentations.

- TECHNICAL MEMORANDUM. Scientific and technical findings that are preliminary or of specialized interest, e.g., quick release reports, working papers, and bibliographies that contain minimal annotation. Does not contain extensive analysis.

- CONTRACTOR REPORT. Scientific and technical findings by NASA-sponsored contractors and grantees.

- CONFERENCE PUBLICATION. Collected papers from scientific and technical conferences, symposia, seminars, or other meetings sponsored or co-sponsored by NASA.

- SPECIAL PUBLICATION. Scientific, technical, or historical information from NASA programs, projects, and missions, often concerned with subjects having substantial public interest.

- TECHNICAL TRANSLATION. English-language translations of foreign scientific and technical material pertinent to NASA's mission.

Specialized services that complement the STI Program Office's diverse offerings include creating custom thesauri, building customized databases, organizing and publishing research results . . . even providing videos.

For more information about the NASA STI Program Office, see the following:

- Access the NASA STI Program Home Page at *http://www.sti.nasa.gov*

- Email your question via the Internet to help@sti.nasa.gov

- Fax your question to the NASA STI Help Desk at (301) 621-0134

- Telephone the NASA STI Help Desk at (301) 621-0390

- Write to:
  NASA STI Help Desk
  NASA Center for AeroSpace Information
  7121 Standard Drive
  Hanover, MD 21076-1320

NASA / TP-2000-210299

An Improved Elastic and Nonelastic Neutron Transport Algorithm for Space Radiation

Martha S. Clowdsley and John W. Wilson
Langley Research Center, Hampton, Virginia

John H. Heinbockel
Old Dominion University, Norfolk, Virginia

R. K. Tripathi, Robert C. Singleterry, Jr., and Judy L. Shinn
Langley Research Center, Hampton, Virginia

National Aeronautics and
Space Administration

Langley Research Center
Hampton, Virginia 23681-2199

July 2000

Available from:

NASA Center for AeroSpace Information (CASI)
7121 Standard Drive
Hanover, MD 21076-1320
(301) 621-0390

National Technical Information Service (NTIS)
5285 Port Royal Road
Springfield, VA 22161-2171
(703) 605-6000

Symbols and Abbreviations

$\mathbf{A}$	coefficient matrix
A_{T_β}	atomic weight
$B[\ ]$	Boltzmann differential operator
C3H10T1/2	mouse embryo cell culture
E_i^*, E_i, E, E'	energy, MeV
$f_{jk,\beta}^d$	direct knockout redistribution, MeV^{-1}
$f_{jk,\beta}^e$	evaporation spectral redistribution, MeV^{-1}
$f_{jk,\beta}^{\text{el}}$	elastic spectral redistribution, MeV^{-1}
H_{ij}, K_{ij}	integral operators
HETC	High Energy Transport Code
HZETRN	High Charge and Energy Transport Code
h	step size for numerical integration
$I_{\text{el}}^{(k)}, I_e^{(k)}, I_d^{(k)}$	integral operators
$I_{s,i}, I_{r,i}, \xi_i$	integrals from E_i to E_{i+1} of terms on right-hand side of Boltzmann equation
LAHET	Los Alamos High Energy Transport Code
MCNP	Monte Carlo N-Particle Transport Code
MCNPX	LAHET/MCNP Code merger
$S_j(E)$	stopping power jth particle
SPE	solar particle event
x_j, y_j, x	depth of penetration of neutron radiation, g/cm^2
$\overline{y} = \text{col}\{\phi_0, \phi_1, \ldots, \phi_{N-1}\}$	column vector of ϕ_i terms
$\gamma_i, m_{ij}, \delta_i$	parameter values
θ	scattering angle
$\theta_1, \theta_2, \theta_1', \theta_2'$	mean value fractions
$\overline{\xi} = \text{col}\{\xi_0, \xi_1, \ldots, \xi_{N-1}\}$	column vector of source terms
ρ_β	number density of β type atoms per unit mass, g particles
$\sigma_j(E)$	total macroscopic cross section per unit mass, cm^2/g
$\sigma_{jk}(E,E')$	macroscopic differential cross section for particle k with energy E' producing particle j with energy E, cm^2/g-MeV particles
$\sigma_{s,\beta}, \sigma_{r,\beta}$	scattering terms, cm^2/g-MeV
σ_β	microscopic cross section, cm^2
$\overline{\sigma}$	average macroscopic cross section, cm^2/g
Φ_i	integral of fluence for ith energy group, neutrons/cm^2
$\phi_e, \phi, \phi_j(E)$	particle fluence, particles/cm^2-MeV

Abstract

A neutron transport algorithm including both elastic and nonelastic particle interaction processes for use in space radiation protection for arbitrary shield material is developed. The algorithm is based upon a multiple energy grouping and analysis of the straight-ahead Boltzmann equation by using a mean value theorem for integrals. The algorithm is then coupled to the Langley HZETRN code through a bidirectional neutron evaporation source term. Evaluation of the neutron fluence generated by the solar particle event of February 23, 1956, for an aluminum-water shield-target configuration is then compared with MCNPX and LAHET Monte Carlo calculations for the same shield-target configuration. With the Monte Carlo calculation as a benchmark, the algorithm developed in this paper showed a great improvement in results over the unmodified HZETRN solution. In addition, a high-energy bidirectional neutron source based on a formula by Ranft showed even further improvement of the fluence results over previous results near the front of the water target where diffusion out the front surface is important. Effects of improved interaction cross sections are modest compared with the addition of the high-energy bidirectional source terms.

Introduction

This paper presents an improved algorithm for the analysis of the transport of secondary neutrons arising in space radiation protection studies. The design and simulation of the operational processes in space radiation shielding and protection require highly efficient computational procedures to adequately characterize time-dependent environments and time-dependent geometric factors and to address shield evaluation issues in a multidisciplinary integrated engineering design environment. One example is the recent study of the biological response in exposures to space solar particle events (SPE's) in which the changing quality of the radiation fields at specific tissue sites are followed over 50 hours of satellite data to evaluate time-dependent factors in biological response of the hematopoietic system (ref. 1). Similarly, the study of cellular repair dependent effects on the neoplastic cell transformation of a C3H10T$\frac{1}{2}$ mouse embryo cell culture population in low Earth orbit, where trapped radiations and galactic cosmic rays vary continuously in intensity and spectral content about the orbital path (ref. 2), requires computationally efficient codes to simulate time-dependent boundary conditions around the orbital path. But even in a steady-state environment which is homogeneous and isotropic, the radiation fields within a spacecraft have large spatial gradients and highly anisotropic factors so that the mapping of the radiation fields within the astronaut's tissues depends on the astronaut timeline of location and orientation within the spacecraft interior where large differences in exposure patterns that depend on the activity of the astronaut have been found (ref. 3). Obvious cases exist where rapid evaluation of exposure fields of specific tissues is required to describe the effects of variations in the time-dependent exterior environment or changing geometric arrangement. A recent study of the time-dependent response factors for 50 hours of exposure to the SPE of August 4, 1972, required 18 CPU hours on a VAX 4000/500 computer by using the nucleon–light ion section of the deterministic high charge and energy transport code HZETRN (ref. 4). In comparison, it is estimated that the related calculation with a standard Monte Carlo code such as HETC (ref. 5) or LAHET (ref. 6), which are restricted to only neutrons, protons, pions, and alphas, would have required approximately 2 years of computer time on a VAX 4000/500 computer. The spacecraft design environment also requires rapid evaluation of the radiation fields to adequately determine effects of multiparameter design changes on system performance (refs. 7 and 8). These effects

are the driving factors in the development and use of deterministic codes and in particular the HZETRN code system which simulates 56 naturally occurring atomic ions and neutrons.

The basic philosophy for the development of the deterministic HZETRN code began with the study by Alsmiller et al. (ref. 5) using an early version of HETC, wherein they demonstrated that the straight-ahead approximation for broad beam exposures was adequate for evaluation of exposure quantities. Wilson and Khandelwal (ref. 9) examined the effects of beam divergence on the estimation of exposure in arbitrary convex geometries and demonstrated that the errors in the straight-ahead approximation are proportional to the square of the ratio of the beam divergence (lateral spread) to the radius of curvature of the shield material. This ratio is small in typical space applications. From a shielding perspective, the straight-ahead approximation overestimates the transmitted flux and the error is found to be small in space radiation exposure quantities. Langley Research Center's first implementation of a numerical procedure was performed by Wilson and Lamkin (ref. 10) as a numerical iterative procedure of the charged components perturbation series expansion of the Boltzmann transport equation and showed good agreement with Monte Carlo calculations for modest penetrations to where neutrons play an important role. The neutron component was added by Lamkin (ref. 11) and closed the gap between the deterministic code and the Monte Carlo code. The resulting code was fast compared with the Monte Carlo codes but still lacked efficiency in generating and operating with large data arrays which would be solved in the next generation of codes.

The transport of high-energy ions is well adapted to the straight-ahead approximation. In fact, the usual assumption that secondary ion fragments are produced with the same velocity as the primary initial ion (ref. 12) is less accurate than the straight-ahead approximation contrary to intuition (ref. 13). The Boltzmann transport equation for the particle fields $\phi_j(x,E)$ is given for the straight-ahead and continuous slowing down approximations as

$$\left[\frac{\partial}{\partial x} - \frac{\partial}{\partial E}S_j(E) + \sigma_j(E)\right] \phi_j(x,E) = \sum_k \int_E^\infty \sigma_{jk}(E,E')\ \phi_k(x,E')\ dE' \qquad (1)$$

where x is the depth of penetration, E is the particle kinetic energy, $S_j(E)$ is the particle stopping power, $\sigma_j(E)$ is the macroscopic interaction cross section, and $\sigma_{jk}(E,E')$ is the macroscopic cross section for particle j of energy E produced as a result of the interaction with particle k of energy E'. It has been customary in codes developed at Langley to invert the differential operator and implement it exactly as a marching procedure (ref. 14). The remaining issue has been to approximate the integral term on the right-hand side of equation (1). The formulation of the code to approximate heavy fragments was facilitated by assuming that their fragment velocity is identical to that of the primary ion velocity. This assumption is inadequate for the description of the coupled nucleonic and light ion components. A computationally compatible nucleonic transport procedure was developed by Wilson et al. (ref. 15) and agreed well with exposure quantities evaluated by Monte Carlo transport procedures (ref. 16). The transport of the nucleonic component was developed by assuming the midpoint energy, within the step size h, was the appropriate energy to evaluate the integral term. Thus, the residual range of the proton will reduce by $h/2$ before the interaction, and the secondary proton residual range will reduce by $h/2$ before arriving at the next marching step. Neutrons show no loss in residual range as their stopping power is zero. This choice was shown to minimize the second-order corrections to the marching procedure (ref. 17). Although reasonable agreement on exposure quantities from Monte Carlo calculations was obtained, the resultant neutron flux at the lowest energies was substantially below the Monte Carlo result in the range of 0.01 to several MeV and required improvement (ref. 18). Analysis revealed that the problem was in the rescattering terms in which the number of elastic scattered neutrons was underestimated numerically, which must be addressed as suggested by Shinn et al. (ref. 18).

The issue of evaluation of the integral term of the Boltzmann equation for the elastic scattering was developed in a prior report (ref. 19). In reference 19, a multiple energy group (multigroup) method based upon a mean value approximation to the integral terms for transporting evaporation neutrons showed vast improvement in the low-energy neutron spectra. Now that the elastic scattering events are adequately represented, consider the addition of improved estimates of nonelastic processes on the neutron transport solution. In the present paper, nonelastic processes are added to the algorithm developed by Heinbockel, Clowdsley, and Wilson (ref. 19). The code is then modified to account for the high-energy neutron production at backward angles. Improved neutron interaction cross sections with less dramatic changes on the neutron spectrum are introduced.

Formulation of Transport Equations

Define the linear differential operator as

$$B[\phi] = \left[\frac{\partial}{\partial x} - \frac{\partial}{\partial E}\ S_j(E) + \sigma_j(E)\right]\ \phi(x,E)$$

$$= \frac{\partial \phi(x,E)}{\partial x} - \frac{\partial}{\partial E}[S_j(E)\ \phi(x,E)] + \sigma_j(E)\ \phi(x,E) \tag{2}$$

and consider the following one-dimensional Boltzmann equation from reference 20

$$B[\phi_j] = \sum_k \int_0^\infty \sigma_{jk}(E,E')\ \phi_k(x,E')\ dE' \tag{3}$$

where ϕ_j is the differential flux spectrum for the type j particles, $S_j(E)$ is the stopping power of the type j particles, and $\sigma_j(E)$ is the total macroscopic cross section. The term $\sigma_{jk}(E,E')$, a macroscopic differential energy cross section for redistribution of particle type and energy, is written as

$$\sigma_{jk}(E,E') = \sum_\beta\ \rho_\beta\ \sigma_\beta(E')\ f_{jk,\beta}(E,E') \tag{4}$$

where $f_{jk,\beta}(E,E')$ is the spectral redistribution, σ_β is a microscopic cross section, and ρ_β is the number density of β type atoms per unit mass of material. The spectral terms are expressed as

$$f_{jk,\beta} = f^{\mathrm{el}}_{jk,\beta} + f^{e}_{jk,\beta} + f^{d}_{jk,\beta} \tag{5}$$

where $f^{\mathrm{el}}_{jk,\beta}$ represents the elastic redistribution in energy, $f^{e}_{jk,\beta}$ represents evaporation terms, and $f^{d}_{jk,\beta}$ represents direct knockout terms. The elastic term is generally limited to a small energy range near that of the primary particle. The evaporation process dominates over the low-energy range ($E < 25$ MeV), and the direct cascading effect dominates over the high-energy range ($E > 25$ MeV), as illustrated in figure 1 with data from reference 20.

Equation (3) is then written for $j = n$ as

$$B[\phi_n] = \sum_k \int_E^\infty \sum_\beta \rho_\beta\ \sigma_\beta(E')\left(f^{\mathrm{el}}_{nk,\beta} + f^{e}_{nk,\beta} + f^{d}_{nk,\beta}\right)\phi_k(x,E')\ dE' \tag{6}$$

which is expanded to the form

$$B[\phi_n] = \int_E^\infty \sum_\beta \rho_\beta \, \sigma_\beta(E') \left(f^{\rm el}_{nn,\beta} + f^e_{nn,\beta} + f^d_{nn,\beta} \right) \phi_n(x,E') \, dE'$$

$$+ \sum_{k \neq n} \int_E^\infty \sum_\beta \rho_\beta \, \sigma_\beta(E') \left(f^{\rm el}_{nk,\beta} + f^e_{nk,\beta} + f^d_{nk,\beta} \right) \phi_k(x,E') \, dE' \tag{7}$$

Define the integral operators as

$$I^{(k)}_{\rm el}[\phi] = \int_E^\infty \sum_\beta \rho_\beta \, \sigma_\beta(E') \, f^{\rm el}_{nk,\beta} \, \phi(x,E') \, dE' \tag{8}$$

$$I^{(k)}_e[\phi] = \int_E^\infty \sum_\beta \rho_\beta \, \sigma_\beta(E') \, f^e_{nk,\beta} \, \phi(x,E') \, dE' \tag{9}$$

$$I^{(k)}_d[\phi] = \int_E^\infty \sum_\beta \rho_\beta \, \sigma_\beta(E') \, f^d_{nk,\beta} \, \phi(x,E') \, dE' \tag{10}$$

where $k = n$ denotes coupling to neutron collisions, $k = p$ denotes the neutron source from proton collisions, and similarly for other ions. When considering only neutrons and protons, equation (7) can be written in the linear operator form as

$$B[\phi_n] = I^{(n)}_{\rm el}[\phi_n] + I^{(n)}_e[\phi_n] + I^{(n)}_d[\phi_n] + I^{(p)}_{\rm el}[\phi_p] + I^{(p)}_e[\phi_p] + I^{(p)}_d[\phi_p] \tag{11}$$

Note that $I^{(p)}_{\rm el}[\phi_p]$ does not contribute to the neutron field because protons cannot produce neutrons through elastic scattering and therefore equation (11), with ϕ_n replaced by ϕ, is written as

$$B[\phi] = I^{(n)}_{\rm el}[\phi] + I^{(n)}_e[\phi] + I^{(n)}_d[\phi] + I^{(p)}_e[\phi_p] + I^{(p)}_d[\phi_p] \tag{12}$$

In reference 19, we assumed the evaporation source to be isotropic and evaluated the transport in forward and backward directions by using the straight-ahead approximation for elastic scattering and found improved agreement with Monte Carlo calculations. The first step in this study is to add effects of nonelastic events into the transport process.

Assume a solution to equation (12) of the form $\phi = \phi_e + \phi_d$, where ϕ_e is the solution for evaporation sources and contributes over the low-energy range and ϕ_d is the solution for the direct knockout sources and contributes mainly over the high-energy range as suggested by figure 1. Substitute this assumed solution into equation (12) and find

$$B[\phi_e] + B[\phi_d] = I^{(n)}_{\rm el}[\phi_e] + I^{(n)}_{\rm el}[\phi_d] + I^{(n)}_e[\phi_e] + I^{(n)}_e[\phi_d]$$

$$+ I^{(n)}_d[\phi_e] + I^{(n)}_d[\phi_d] + I^{(p)}_e[\phi_p] + I^{(p)}_d[\phi_p] \tag{13}$$

In reference 19, the terms $I^{(n)}_e[\phi_e]$ and $I^{(n)}_d[\phi_e]$ were set to zero to consider only elastic scattering. This allows estimates of the elastic scattering effects on the transport of evaporation neutrons. In contrast, these terms are retained and they demonstrate nonelastic effects on the transport of evaporated neutrons. This change also allows flexibility in further improving the HZETRN code as shown later in this report. As in reference 19, we assume that ϕ_d was calculated by the

HZETRN program because for the direct cascade neutrons the straight-ahead approximation is valid. Consequently, ϕ_d is a solution of the equation

$$B[\phi_d] = I_{\rm el}^{(n)}[\phi_d] + I_d^{(n)}[\phi_d] + I_d^{(p)}[\phi_p] \tag{14}$$

This assumption simplifies equation (13) to the form

$$B[\phi_e] = I_{\rm el}^{(n)}[\phi_e] + I_e^{(n)}[\phi_e] + I_d^{(n)}[\phi_e] + I_e^{(n)}[\phi_d] + I_e^{(p)}[\phi_p] \tag{15}$$

The elastic and reaction scattering terms are defined as

$$\sigma_{s,\beta} = \rho_\beta \ \sigma_\beta(E') \ f_{nk,\beta}^{\rm el}(E,E')$$

$$\sigma_{r,\beta} = \rho_\beta \ \sigma_\beta(E') \left[f_{nk,\beta}^{e}(E,E') + f_{nk,\beta}^{d}(E,E') \right]$$

with units of cm^2/g-MeV, and for neutrons the stopping power $S_j(E)$ is assumed zero, and therefore, equation (15) reduces to the integro-differential transport equation with source term as

$$\left[\frac{\partial}{\partial x} + \sigma(E) \right] \phi_e(x,E) = \sum_\beta \int_E^\infty \left[\sigma_{s,\beta}(E,E') + \sigma_{r,\beta}(E,E') \right] \ \phi_e(x,E') \ dE' + g(E,x) \tag{16}$$

Equation (16) represents the steady state evaporation neutron fluence $\phi_e(x,E)$ at depth x and energy E. The various terms in equation (16) are energy E with units of MeV, depth in medium is x with units of g/cm^2, $\phi_e(x,E)$ (in particles/cm^2-MeV) is the evaporation neutron fluence, and $g(E,x) = I_e^{(n)}[\phi_d] + I_e^{(p)}[\phi_p]$ (in particles/g-MeV) is a volume source term to be evaluated by the HZETRN algorithm. Equation (16) is further reduced by considering the neutron energies before and after an elastic collision. The neutron energy E after an elastic collision with a nucleus of mass number A_{T_β}, initially at rest, is from reference 21

$$E = E' \left[\frac{A_{T_\beta}^2 + 2A_{T_\beta}\cos\theta + 1}{\left(A_{T_\beta} + 1 \right)^2} \right] \tag{17}$$

where E' is the neutron energy before the collision, A_{T_β} is the atomic weight of the βth type of atom being bombarded, and θ is the angle of scatter. Note that for forward scattering $\theta = 0$, $E = E'$, and for backward scattering $\theta = \pi$, $E = E'\alpha_\beta$, where α_β is the ratio

$$\alpha_\beta = \left(\frac{A_{T_\beta} - 1}{A_{T_\beta} + 1} \right)^2 \tag{18}$$

which is a constant less than 1. Therefore, change the limits of integration for the elastic scattering term in equation (16) to $[E,E/\alpha_\beta]$, which represents the kinetically allowed energies for the scattered neutron to result in an energy E. Equation (16) then is written as

$$\left[\frac{\partial}{\partial x} + \sigma(E) \right] \phi_e(x,E) = \sum_\beta \int_E^{E/\alpha_\beta} \sigma_{s,\beta}(E,E') \ \phi_e(x,E') \ dE'$$

$$+ \sum_\beta \int_E^\infty \sigma_{r,\beta}(E,E') \ \phi_e(x,E') \ dE' + g(E,x) \tag{19}$$

The quantity $\sigma(E)$ has units of cm^2/g and is a macroscopic cross section given by

$$\sigma(E) = \sum_\beta \rho_\beta \ \sigma_\beta^{\mathrm{el}}(E) + \sum_\beta \rho_\beta \ \sigma_\beta^r(E) \tag{20}$$

where ρ_β is the number of atoms per gram, $\sigma_\beta^{\mathrm{el}}(E)$ is a microscopic elastic cross section in units of $\mathrm{cm}^2/\mathrm{atom}$, and $\sigma_\beta^r(E)$ is the corresponding reaction cross section. Other units for equation (16) are obtained from the previous units by using the scale factor representing the density of the material in units of g/cm^3.

Mean Value Theorem

Throughout the remaining discussions the following mean value theorem is used for integrals.

Mean Value Theorem: For $\phi(x,E)$ and $f(E)$ continuous over an interval $a \le E \le b$ such that (1) $\phi(x,E)$ does not change sign over the interval (a,b), (2) $\phi(x,E)$ is integrable over the interval (a,b), and (3) $f(E)$ is bounded over the interval (a,b), then there exists at least one point ϵ such that

$$\int_a^b f(E) \ \phi(x,E) \ dE = f(\epsilon) \int_a^b \phi(x,E) \ dE \qquad (a \le \epsilon \le b) \tag{21}$$

In particle transport this mean value approach is not commonly used. In reactor neutron calculations, an assumed spectral dependence for $\phi(x,E)$ is used to approximate the integral over energy groups. The present use of the mean value theorem is free of this assumption; thus, more flexibility is allowed in the HZETRN code, and the result is a fast and efficient algorithm for low-energy neutron analysis.

Multigroup Method

To solve equation (19), partition the energy domain into a set of energies $\{E_0, E_1, \ldots, E_i, E_{i+1}, \ldots\}$. Consider first the case where there is only one value of β which represents neutron penetration into a single element material and let ϕ_e be denoted by ϕ. Equation (19) is integrated from E_i to E_{i+1} with respect to the energy E to obtain

$$\int_{E_i}^{E_{i+1}} \frac{\partial \phi(x,E)}{\partial x} \ dE + \int_{E_i}^{E_{i+1}} \sigma(E) \ \phi(x,E) \ dE = I_{s,i} + I_{r,i} + \xi_i \tag{22}$$

where

$$I_{s,i} = \int_{E_i}^{E_{i+1}} \int_E^{E/\alpha} \sigma_s(E,E') \ \phi(x,E') \ dE' \ dE \tag{23}$$

$$I_{r,i} = \int_{E_i}^{E_{i+1}} \int_E^{\infty} \sigma_r(E,E') \ \phi(x,E') \ dE' \ dE \tag{24}$$

$$\xi_i = \int_{E_i}^{E_{i+1}} g(E,x) \ dE \tag{25}$$

The quantity

$$\Phi_i(x) = \int_{E_i}^{E_{i+1}} \phi(x,E) \ dE \tag{26}$$

is associated with the ith energy group (E_i, E_{i+1}), so that $\frac{1}{E_{i+1}-E_i}\Phi_i(x)$ represents an average fluence for the ith energy group. Then equation (22) can be written as an ordinary differential equation in terms of $\Phi_i(x)$ as follows. In the first term in equation (22), interchange the order of integration and differentiation to obtain

$$\int_{E_i}^{E_{i+1}} \frac{\partial \phi(x,E)}{\partial x}\, dE = \frac{d\Phi_i(x)}{dx} \tag{27}$$

By using the previously stated mean value theorem for integrals, the second term in equation (22) can be expressed as

$$\int_{E_i}^{E_{i+1}} \sigma\ \phi(x,E)\ dE = \overline{\sigma}\ \Phi_i(x) \tag{28}$$

where $\overline{\sigma} = \sigma[E_i + \theta(E_{i+1} - E_i)]$ is a mean value associated with some value of θ between 0 and 1.

For the term $I_{s,i}$ in equation (23), interchange the order of integration as illustrated in figure 2. The integration of equation (23) depends upon the energy partition selected. For example, figure 2(b) illustrates an energy partition where $E_{i+1} < E_i/\alpha$; for this case we can write equation (23) as

$$\begin{aligned} I_{s,i} = &\int_{E'=E_i}^{E_{i+1}} \int_{E=E_i}^{E'} H_s\ dE\ dE' + \int_{E'=E_{i+1}}^{E_i/\alpha} \int_{E=E_i}^{E_{i+1}} H_s\ dE\ dE' \\ &+ \int_{E'=E_i/\alpha}^{E_{i+1}/\alpha} \int_{E=\alpha E'}^{E_{i+1}} H_s\ dE\ dE' \end{aligned} \tag{29}$$

where $H_s = \sigma_s(E,E')\ \phi(x,E')$. Figure 2(c) depicts the case where $E_{i+1} = E_i/\alpha$ exactly for all i. In this special case, equation (23) reduces to

$$I_{s,i} = \int_{E'=E_i}^{E_{i+1}} \int_{E=E_i}^{E'} H_s\ dE\ dE' + \int_{E'=E_{i+1}}^{E_{i+1}/\alpha} \int_{E=\alpha E'}^{E_{i+1}} H_s\ dE\ dE' \tag{30}$$

The selection of an energy partition can lead to two or more distinct energy groups associated with each interchange in the order of integration. For example, see figure 3(a).

The evaluation of equation (24) is somewhat more complicated. As an approximation, we assume there is an energy E_N such that $\phi(x,E)$ can be taken as zero for all $E > E_N$. In this case, equation (24) can be written as

$$I_{r,i} = \int_{E'=E_i}^{E_{i+1}} \int_{E=E_i}^{E'} H_r\ dE\ dE' + \sum_{j=i+1}^{N-1} \int_{E_j}^{E_{j+1}} \int_{E_i}^{E_{i+1}} H_r\ dE\ dE' \tag{31}$$

where $H_r = \sigma_r(E,E')\ \phi(x,E')$. For example see figure 3(b).

Equations (30) and (31) may then be written for the case where $E_{i+1} = E_i/\alpha$ as

$$I_{s,i} = \int_{E_i}^{E_i^*} \sigma_s(E,E_i^*)\ dE\ \Phi_i(x)\ dE + \int_{\alpha E_{i+1}^*}^{E_{i+1}} \sigma_s(E,E_{i+1}^*)\ dE\ \Phi_{i+1}(x)\ dE \tag{32}$$

and

$$I_{r,i} = \int_{E_i}^{E_i^*} \sigma_r(E,E_i^*)\ dE\ \Phi_i(x)\ dE + \sum_{j=i+1}^{N-1} \int_{E_i}^{E_{i+1}} \sigma_r(E,E_j^*)\ dE\ \Phi_j(x)\, dE \tag{33}$$

where $E_i^* = \theta_1(E_{i+1} - E_i)$ and $E_{i+1} = \theta_2(E_{i+2} - E_{i+1})$ for some θ_1 and θ_2 such that $0 < \theta_1, \theta_2 < 1$ by once again using the previously stated mean value theorem. The special partitioning of the energy as illustrated in figure 2(c) enables us to obtain from equation (22) a system of ordinary differential equations of the form

$$\frac{d}{dx}\begin{bmatrix} \Phi_0 \\ \Phi_1 \\ \vdots \\ \vdots \\ \Phi_{N-1} \end{bmatrix} = \begin{bmatrix} a_{11} & a_{12} & a_{13} & \cdots & a_{1N} \\ & a_{22} & a_{23} & \cdots & a_{2N} \\ & & a_{33} & \cdots & \vdots \\ & -0- & & \ddots & \vdots \\ & & & & a_{NN} \end{bmatrix} \begin{bmatrix} \Phi_0 \\ \Phi_1 \\ \vdots \\ \vdots \\ \Phi_{N-1} \end{bmatrix} + \begin{bmatrix} \xi_0 \\ \xi_1 \\ \vdots \\ \vdots \\ \xi_{N-1} \end{bmatrix} \tag{34}$$

where each equation is associated with an energy group. This is where the term multigroup method originates. In equation (34), the coefficient matrix has the elements

$$a_{i,i} = \int_{E_i}^{E_i^*} [\sigma_s(E, E_i^*) + \sigma_r(E, E_i^*)]\, dE - \sigma(E_i^*)$$

$$a_{i,i+1} = \int_{\alpha E_{i+1}^*}^{E_{i+1}} \sigma_s(E, E_{i+1}^*)\, dE + \int_{E_{i+1}}^{E_{i+2}} \sigma_r(E, E_{i+1}^*)\, dE$$

$$a_{i,i+j} = \int_{E_{i+j}}^{E_{i+j+1}} \sigma_r(E, E_{i+j}^*)\, dE \qquad (j = 2, 3, \ldots)$$

Further assume that for some large value of N, Φ_i equals 0 for all $i \geq N$. This assumption gives rise to the following system of ordinary differential equations:

$$\frac{d\overline{y}}{dx} = \mathbf{A}\overline{y} + \overline{\xi}$$

subject to the initial conditions $\overline{y}(0) = \overline{0}$. Here $\overline{y}$ is the column vector of Φ_i values, $\mathrm{col}(\Phi_0, \Phi_1, \ldots, \Phi_{N-1})$, the matrix $\mathbf{A}$ is an N by N upper triangular matrix, and $\overline{\xi}$ is the column vector $\mathrm{col}(\xi_0, \xi_1, \ldots, \xi_{N-1})$. This system can be solved by using back substitution. In a similar manner, the integrals in equation (29) and (31) can be evaluated for other kinds of energy partitioning, and a system of equations having the same form of equation (34) obtained. How the elements of the matrix $\mathbf{A}$ are calculated will depend upon the elastic scattering as determined by the type of energy partition. (See, for example, fig. 3(a).)

For our purposes the system of equations (eq. (34)) is used to discuss some of the problems associated with the multigroup method. Of prime concern is how an energy grid is to be constructed and how this energy grid controls the size of the matrix in equation (34). Consider the construction of the energy partition

$$\left\{ E_0, \frac{E_0}{\alpha}, \frac{E_0}{\alpha^2}, \ldots, \frac{E_0}{\alpha^N} \right\}$$

where $E_0 = 0.1$ MeV, for the selected elements of lithium, aluminum, and lead. Table 1 illustrates integer values of N necessary to achieve energies greater than 30 MeV. These values of N represent the size of the matrix associated with the number of energy groups. The value $E_0 = 0.1$ MeV, in terms of human exposure, represents a lower bound where lower energies are not important. The value of 30 MeV represents an upper limit for the evaporation particles and could be adjusted for other source terms.

Table 1. Energy Partition Size N

Element	α	N	$0.1/\alpha^N$
Lithium	0.563	10	31.53
Aluminum	0.862	39	32.75
Lead	0.981	298	30.38

Observe that for energy partitions where $E_{i+1} < E_i/\alpha$ the values of N are larger, and if $E_{i+1} > E_i/\alpha$ the values of N are smaller. The cases where $E_{i+1} > E_i/\alpha$ give rise to problems associated with the integration of the elastic scattering terms over the areas A_1 and A_2 of figure 2(d) when the order of integration is interchanged. In this figure, the area A_1 is associated with the integral defining Φ_i, and the area A_2 is a remaining area associated with an integral which is some fraction of the integral defining Φ_{i+1} which is outside the range of integration; therefore, some approximation must be made to define this fractional part. This type of partitioning produces errors, due to any approximations, but it has the advantage of greatly reducing the size of the N by N matrix $\mathbf{A}$ at the cost of introducing errors into the system of equations. A more detailed analysis of the energy partition can be found in reference 22.

The case of neutron penetration into a composite material gives rise to the case where there is more than one value of β in equation (16). In this special case, equation (23) becomes

$$I_{s,i} = \sum_{\beta} \int_{E_i}^{E_{i+1}} \int_{E}^{E/\alpha_\beta} \sigma_{s,\beta}(E,E')\ \phi(x,E')\ dE'\ dE \tag{35}$$

and equation (24) becomes

$$I_{r,i} = \sum_{\beta} \int_{E_i}^{E_{i+1}} \int_{E}^{\infty} \sigma_{r,\beta}(E,E')\ \phi(x,E')\ dE'\ dE \tag{36}$$

In order to avoid the errors introduced when an energy grid is selected such that $E_{i+1} > E_i/\alpha$, we select $\alpha = \max(\alpha_1, \alpha_2, \ldots, \alpha_\beta)$ and construct the energy partition where $E_{i+1} = E_i/\alpha$ so that $E_{i+1} \leq E_i/\alpha_\beta$ for all β. Obtain a system of differential equations having the same upper triangular form but with elastic scattering contributions for off-diagonal elements. Observe that for some arbitrary energy grouping we have, for the element hydrogen, a case where the value of α_β is zero and E_i/α_β is therefore infinite. In this situation, we must integrate over many energy groups. In this case, the area of integration is similar to that shown in figure 3(b). For any composite material, depending upon the selected energy partitioning, some type of approximations must be made when the order of integration is interchanged in equation (35). Also the problem of selecting the mean values associated with each of these integrations exists and now addressed.

Mean Value Determination

A realistic test case was solved analytically and numerically (with and without the multigroup approximation) for which the mean values were found empirically for several single element materials (ref. 19). The values determined are

$$E_i^* = E_i + \theta_1(E_{i+1} - E_i)$$

$$E_{i+1}^* = E_{i+1} + \theta_2(E_{i+2} - E_{i+1})$$

where

$$\theta_1 = \begin{cases} \gamma_1 + m_{11}(E - E_{11}) - \delta_1 & (E > E_{11}) \\ \gamma_1 + m_{12}(E - E_{11}) - \delta_1 & (E_{22} < E < E_{11}) \\ \gamma_3 + m_{13}(E - E_{22}) - \delta_1 & (E < E_{22}) \end{cases}$$

and

$$\theta_2 = \begin{cases} \gamma_2 + m_{21}(E - E_{11}) & (E > E_{11}) \\ \gamma_2 + m_{22}(E - E_{11}) & (E_{22} < E < E_{11}) \\ \gamma_4 + m_{23}(E - E_{22}) & (E < E_{22}) \end{cases}$$

where

$$\gamma_1 = 0.93 \qquad m_{11} = 0.0030485 \qquad m_{21} = 0.004355$$
$$\gamma_2 = 0.90 \qquad m_{12} = 0.2490258 \qquad m_{22} = 0.249026$$
$$\gamma_3 = 0.30 \qquad m_{13} = -0.3937186 \qquad m_{23} = -0.255920$$
$$\gamma_4 = 0.27 \qquad E_{11} = 3.037829 \qquad E_{22} = 0.5079704$$

and δ_1 is 0.0 for lead, 0.02 for aluminum, and 0.075 for lithium. These values of θ for the mean value theorems were determined by trial and error so that the multigroup curves would have the correct shape and agree with the numerical solution. These selections for the mean values are not unique.

Application to Evaporation Source in Al-H_2O Shield-Target Configuration

Apply the previous development to an application of the multigroup method associated with an aluminum-water shield-target configuration. In particular, consider the case where the source term $g(E,x)$, in equation (16), represents evaporation neutrons produced per unit mass per MeV and is specified as a numerical array of values corresponding to various shield-target thicknesses and energies. The numerical array of values is produced by the radiation code HZETRN developed by Wilson et al. (ref. 4). This numerical array of source term values is actually given in the form $g(E_i,x_j,y_k)$ in units of particles/g-MeV, where y_k represents discrete values for various target thicknesses of water in g/cm^2, x_j represents discrete values for various shield thicknesses of aluminum, also in units of g/cm^2, and E_i represents discrete energy values in units of MeV. These discrete source term values are used in the following way. Consider first the solution of equation (16) by the multigroup method for an all-aluminum shield with no target material, that is, target thickness $y_k = 0$. The HZETRN program was run to simulate the solar particle event of February 23, 1956, and the source term $g(E_i,x_j,y_k)$ associated with an aluminum-water shield-target configuration was generated for these conditions. Using this source term, we solved equation (16) by the multigroup method.

For a single shield material with only one value of β, equation (16) becomes

$$\left[\frac{\partial}{\partial x} + \sigma(E)\right] \phi(x,E) = \int_E^{E/\alpha} \sigma_s(E,E')\, \phi(x,E')\, dE' + \int_E^{\infty} \sigma_r(E,E')\, \phi(x,E')\, dE' + g(E,x) \tag{37}$$

where an integration of equation (37) from E_i to E_{i+1} produces

$$\begin{aligned}
&\int_{E_i}^{E_{i+1}} \frac{\partial \phi}{\partial x}\, dE + \int_{E_i}^{E_{i+1}} \sigma(E)\ \phi(x,E)\ dE \\
&\quad = \int_{E_i}^{E_{i+1}} \int_{E}^{E/\alpha} \sigma_s(E,E')\ \phi(x,E')\ dE'\ dE \\
&\qquad + \int_{E_i}^{E_{i+1}} \int_{E}^{\infty} \sigma_r(E,E')\ \phi(x,E')\ dE'\ dE + \int_{E_i}^{E_{i+1}} g(E,x)\ dE
\end{aligned} \tag{38}$$

We define the quantities

$$\left.\begin{aligned}
\Phi_i &= \int_{E_i}^{E_{i+1}} \phi(x,E)\ dE \\
\xi_i &= \int_{E_i}^{E_{i+1}} g(E,x)\ dE
\end{aligned}\right\} \tag{39}$$

and interchange the order of integration of the double integral terms in equation (38). If the energy grid is chosen so that $E_{i+1} = E_i/\alpha$, a mean value theorem is applied to obtain the result

$$\begin{aligned}
\frac{d\Phi_i}{dx} + \overline{\sigma}\Phi_i = &\int_{E_i}^{E_{i+1}} \int_{E=E_i}^{E'} \sigma_s(E,E')\ dE\ \phi(x,E')\ dE' \\
&+ \int_{E_{i+1}}^{E_{i+2}} \int_{E=\alpha_1 E'}^{E_{i+1}} \sigma_s(E,E')\ dE\ \phi(x,E')\ dE' \\
&+ \int_{E_i}^{E_{i+1}} \int_{E=E_i}^{E'} \sigma_r(E,E')\ dE\ \phi(x,E')\ dE' \\
&+ \sum_{j=i+1}^{N-1} \int_{E_j}^{E_{j+1}} \int_{E_i}^{E_{i+1}} \sigma_r(E,E')\ dE\ \phi(x,E')\ dE' + \xi_i
\end{aligned} \tag{40}$$

over the energy group $E_i < E' < E_{i+1}$. The first double integral in equation (40) represents integration over the lower triangle illustrated in figure 2(c). The second double integral in equation (40) represents integration over the upper triangle illustrated in figure 2(c). Define

$$\left.\begin{aligned}
g_1(E') &= \int_{E=E_i}^{E'} \sigma_s(E,E')\ dE \\
g_2(E') &= \int_{E=\alpha_1 E'}^{E_{i+1}} \sigma_s(E,E')\ dE
\end{aligned}\right\} \tag{41}$$

and

$$\left.\begin{aligned}
r_1(E') &= \int_{E=E_i}^{E'} \sigma_r(E,E')\ dE \\
r_{2i,m}(E'_m) &= \int_{E_i}^{E_{i+1}} \sigma_r(E,E'_m)\ dE
\end{aligned}\right\} \tag{42}$$

then employ another application of a mean value theorem for integrals to write equation (40) in the form

$$\frac{d\Phi_i}{dx} + \overline{\sigma}\,\Phi_i = g_1\left[E_i + \theta_1(E_{i+1} - E_i)\right]\Phi_i + g_2\left[E_{i+1} + \theta_2(E_{i+2} - E_{i+1})\right]\Phi_{i+1}$$

$$+ r_1\left[E_i + \theta_1(E_{i+1} - E_i)\right]\Phi_i + \sum_{j=i+1}^{N-1} r_{2i,j}\left[E_j + \theta_2(E_{j+1} - E_j)\right]\Phi_j + \xi_i \qquad (43)$$

This produces the matrix coefficients associated with the energy group E_i to E_{i+1} so that

$$\left.\begin{aligned} a_{i,i} &= g_1 + r_1 - \overline{\sigma} \\ a_{i,i+1} &= g_2 + r_{2i,i+1} \\ a_{i,i+j} &= r_{2i,i+j} \end{aligned}\right\} \qquad (j = 2, 3, \ldots) \qquad (44)$$

In this way, the diagonal and off-diagonal elements of the coefficient matrix in equation (37) are calculated.

For a compound target material made up of more than one type of atom, *we* modify slightly the solution technique given in reference 19. For a target material comprised of component 1 and component 2, there are two values for α. A value α_1 is determined for component 1 and a value α_2 is determined for component 2 of the compound material. In this case, equation (37) takes on the form

$$\left[\frac{\partial}{\partial x} + \sigma(E)\right]\phi(x,E) = \int_E^{E/\alpha_1} \sigma_{s_1}(E,E')\,\phi(x,E')\,dE'$$

$$+ \int_E^{E/\alpha_2} \sigma_{s_2}(E,E')\,\phi(x,E')\,dE' + \int_E^{\infty} \sigma_{r_1}(E,E')\,\phi(x,E')\,dE'$$

$$+ \int_E^{\infty} \sigma_{r_2}(E,E')\,\phi(x,E')\,dE' + g(E,x) \qquad (45)$$

where σ_{s1} and σ_{s2} are scattering terms and σ_{r_1} and σ_{r_2} are reaction terms associated with the respective components of the compound material. These terms are calculated in the HZETRN code. We consider two cases. Case I requires that the E/α_2 line be above the E/α_1 line. In case II, α_2 equals 0 (the hydrogen case), and the limit of integration for the second integral goes to infinity. Each case is considered separately.

For case I, we assume that $\alpha_1 > \alpha_2 > 0$ and select the energy spacing $E_{i+1} = E_i/\alpha_1$. We then proceed as we did using the single component shield material. Integrate equation (45) from E_i to E_{i+1} and interchange the order of integration on the double integral terms. Define $\xi_i = \int_{E_i}^{E_{i+1}} g(E,x)\,dE$ and obtain the equation

$$\frac{d\Phi_i}{dx} + \overline{\sigma}\,\Phi_i = H_{11} + H_{12} + H_{21} + H_{22} + K_{11} + K_{12} + K_{21} + K_{22} + \xi_i \qquad (46)$$

where $H_{\beta 1}$ and $H_{\beta 2}$ represent the elastic scattering caused by collisions with β type atoms and $K_{\beta 1}$ and $K_{\beta 2}$ represent the nonelastic scattering. Note that $H_{\beta 1}$ and $K_{\beta 1}$ are integrals over the energy range (E_i, E_{i+1}) for $\beta = 1, 2$, and $H_{\beta 2}$ and $K_{\beta 2}$ represent integrals over higher energies.

The integrals H_{11}, H_{12}, K_{11}, and K_{12} are the easiest to evaluate because of the exact spacing of the energy partition. These integrals have the forms

$$H_{11} = \int_{E_i}^{E_{i+1}} \int_{E=E_i}^{E'} \sigma_{s1}(E,E')\ dE\ \phi(x,E')\ dE' \tag{47}$$

$$H_{12} = \int_{E_{i+1}}^{E_{i+2}} \int_{E=\alpha_1 E'}^{E_{i+1}} \sigma_{s1}(E,E')\ dE\ \phi(x,E')\ dE' \tag{48}$$

and

$$K_{11} = \int_{E_i}^{E_{i+1}} \int_{E=E_i}^{E'} \sigma_{r1}(E,E')\ dE\ \phi(x,E')\ dE' \tag{49}$$

$$K_{12} = \sum_{j=i+1}^{N-1} \int_{E_j}^{E_{j+1}} \int_{E_i}^{E_{i+1}} \sigma_{r1}(E,E')\ dE\ \phi(x,E')\ dE' \tag{50}$$

Here the first subscript represents the material component. A second subscript of 1 represents integration over the lower triangle in figure 2(c). A second subscript of 2 represents integration over upper triangles, like figure 2(c), or higher rectangles, like figures 3(a) and (b). Defining the terms

$$h_{1(\beta)}(E') = \int_{E=E_i}^{E'} \sigma_{s,\beta}(E,E')\ dE \qquad (\beta = 1,2) \tag{51}$$

$$h_{2(1)}(E') = \int_{E=\alpha_1 E'}^{E_{i+1}} \sigma_{s,1}(E,E')\ dE \tag{52}$$

$$k_{1(\beta)}(E') = \int_{E=E_i}^{E'} \sigma_{r,\beta}(E,E')\ dE \qquad (\beta = 1,2) \tag{53}$$

$$k_{2(\beta)}(E') = \int_{E=E_i}^{E_{i+1}} \sigma_{r,\beta}(E,E')\ dE \qquad (\beta = 1,2) \tag{54}$$

and using the mean value theorem for integrals we obtain from equations (47) through (50)

$$\left.\begin{aligned} H_{11} &= h_{1(1)}[E_i + \theta_1(E_{i+1} - E_i)]\Phi_i \\ H_{12} &= h_{2(1)}[E_{i+1} + \theta_2(E_{i+2} - E_{i+1})]\Phi_{i+1} \\ K_{11} &= k_{1(1)}[E_i + \theta_1'(E_{i+1} - E_i)]\Phi_i \\ K_{12} &= \sum_{j=i+1}^{N-1} k_{2(1)}[E_j + \theta_2'(E_{j+1} - E_j)]\Phi_j \end{aligned}\right\} \tag{55}$$

where θ_1,θ_2 and θ_1',θ_2' define intermediate energy values associated with the mean value theorem.

The integrals H_{21} and H_{22} are associated with integration limits $(E,E/\alpha_2)$ and energy intervals dictated by the selection of α_1 for determining the energy spacings. The integral H_{21} is associated with the triangular area shown in figure 3(a) and takes the form

$$H_{21} = \int_{E_i}^{E_{i+1}} \int_{E=E_i}^{E'} \sigma_{s_2}(E,E')\ dE\ \phi(x,E')\ dE' \tag{56}$$

The integral H_{22} is associated with the remaining shaded area shown in figure 3(a). This remaining area is made up of a number of rectangles, trapezoids, and triangles. We approximate the integral over each of these rectangles, trapezoids, and triangles as a fraction η_j of the integral over the whole rectangle with area $A_{ij} = (E_{i+1} - E_i)(E_{j+1} - E_j)$. Integral H_{22}, therefore, takes the form

$$H_{22} = \sum_{j=i+1}^{N-1} \eta_j \int_{E_j}^{E_{j+1}} \int_{E_i}^{E_{i+1}} \sigma_{s_2}(E,E')\ dE\ \phi(x,E')\ dE' \tag{57}$$

where

$$\eta_j = \left\{ \begin{array}{cc} 1 & \left(E_{j+1} < \frac{E_i}{\alpha_2}\right) \\ \frac{A_{ij} - 0.5(\alpha_2 E_{j+1} - E_i)(E_{j+1} - E_i/\alpha_2)}{A_{ij}} & \left(E_j < \frac{E_i}{\alpha_2} < E_{j+1}\right) \\ \frac{0.5[(E_{i+1} - \alpha_2 E_{j+1}) + (E_{i+1} - \alpha_2 E_j)](E_{j+1} - E_j)}{A_{ij}} & \left(\frac{E_i}{\alpha_2} < E_j < E_{j+1} < \frac{E_{j+1}}{\alpha_2}\right) \\ \frac{0.5(E_{i+1}/\alpha_2 - E_j)(E_{i+1} - \alpha_2 E_j)}{A_{ij}} & \left(\frac{E_i}{\alpha_2} < E_j < \frac{E_{i+1}}{\alpha_2} < E_{j+1}\right) \\ 0 & \left(\frac{E_{i+1}}{\alpha_2} < E_j\right) \end{array} \right\} \tag{58}$$

Defining the term

$$h_{3(2)}(E') = \int_{E=E_i}^{E_{i+1}} \sigma_{s,2}(E,E')\ dE \tag{59}$$

H_{21} and H_{22} can be written as

$$\left. \begin{array}{l} H_{21} = h_{1(2)} \Phi_i \\ H_{22} = \sum_{j=i+1}^{N-1} \eta_j h_{3(2)} \Phi_j \end{array} \right\} \tag{60}$$

Similar to K_{11} and K_{12}, integrals K_{21} and K_{22} are given by

$$\left. \begin{array}{l} K_{21} = k_{1(2)} \Phi_i \\ K_{22} = \sum_{j=i+1}^{N-1} k_{2(2)} \Phi_j \end{array} \right\} \tag{61}$$

The coefficients for our system of differential equations (eq. (34)) are then given by

$$\left. \begin{array}{l} a_{i,i} = h_{1(1)} + h_{1(2)} + k_{1(1)} + k_{1(2)} - \overline{\sigma} \\ a_{i,i+1} = h_{2(1)} + \eta_{i+1} h_{3(2)} + k_{2(1)} + k_{2(2)} \\ a_{i,i+2} = \eta_{i+2} h_{3(2)} + k_{2(1)} + k_{2(2)} \\ a_{i,i+3} = \eta_{i+3} h_{3(2)} + k_{2(1)} + k_{2(2)} \\ \vdots \end{array} \right\} \tag{62}$$

where evaluation at the appropriate mean energies is implied.

In case II, the second component is hydrogen which means that $\alpha_2 = 0$; therefore, one of the limits of integration becomes infinite. We once again let α_1 determine the energy spacing and integrate equations (47) through (50) over an energy interval (E_i, E_{i+1}) which is determined by the $E' = E/\alpha_1$ line. Using the definitions given by equations (39) we integrate equation (45) over the interval (E_i, E_{i+1}) and then interchange the order of integration in the resulting double integrals to obtain

$$\frac{d\Phi_i}{dx} + \overline{\sigma}\Phi_i = H_1^* + H_2^* + K_1^* + K_2^* + \xi_i \tag{63}$$

where

$$H_1^* = \int_{E_i}^{E_{i+1}} \int_{E=E_i}^{E'} \sigma_{s_1}(E,E')\ dE\ \phi(x,E')\ dE' + \int_{E_{i+1}}^{E_{i+2}} \int_{E=\alpha_1 E'}^{E_{i+1}} \sigma_{s_1}(E,E')\ dE\ \phi(x,E')\ dE' \tag{64}$$

$$H_2^* = \int_{E_i}^{E_{i+1}} \int_{E_i}^{E'} \sigma_{s_2}(E,E')\ dE\ \phi(x,E')\ dE' + \sum_{j=1}^{N} \int_{E_{i+j}}^{E_{i+j+1}} \int_{E_i}^{E_{i+1}} \sigma_{s_2}(E,E')\ dE\ \phi(x,E')\ dE' \tag{65}$$

$$K_\beta^* = \int_{E_i}^{E_{i+1}} \int_{E_i}^{E'} \sigma_{r,\beta}(E,E')\ dE\ \phi(x,E')\ dE' + \sum_{j=1}^{N} \int_{E_{i+j}}^{E_{i+j+1}} \sigma_{r,\beta}(E,E')\ dE\ \phi(x,E')\ dE' \tag{66}$$

where for all N^* greater than some integer $N > 0$, we know that $\phi(x,E)$ will be taken as zero. Define

$$h_4(E') = \int_{E_i}^{E'} \sigma_{s_1}(E,E')\ dE \qquad (E_i < E' < E_{i+1}) \tag{67}$$

$$h_5(E') = \int_{\alpha_1 E'}^{E_{i+1}} \sigma_{s_1}(E,E')\ dE \qquad (E_{i+1} < E' < E_{i+2}) \tag{68}$$

$$h_6(E') = \int_{E_i}^{E'} \sigma_{s_2}(E,E')\ dE \qquad (E_i < E' < E_{i+1}) \tag{69}$$

$$h_{7(j)}(E') = \int_{E_{i+j}}^{E_{i+j+1}} \sigma_{s_2}(E,E')\ dE \qquad (E_{i+j} < E'_j < E_{i+j+1}) \tag{70}$$

$$k_{3(\beta)}(E') = \int_{E_i}^{E'} \sigma_{r,\beta}(E,E')\ dE \tag{71}$$

$$k_{4(\beta)}(E') = \int_{E_i}^{E_{i+1}} \sigma_{r,\beta}(E,E')\ dE \tag{72}$$

then write the coefficients associated with the system of differential equations as

$$\left.\begin{aligned} a_{i,i} &= h_4 + h_6 + k_{3(1)} + k_{3(2)} - \overline{\sigma} \\ a_{i,i+1} &= h_5 + h_{7(1)} + k_{4(1)} + k_{4(2)} \\ a_{i,i+2} &= h_{7(2)} + k_{4(1)} + k_{4(2)} \\ &\vdots \end{aligned}\right\} \tag{73}$$

where evaluation at the appropriate mean energies is implied.

In this way, we generate a system of equations having the triangular form given by equation (34). We again use the source terms $g(E_i,x_j,y_k)$ obtained from the HZETRN simulation of the solar particle event of February 23, 1956, associated with an aluminum-water shield-target configuration. Note that now we must solve the multigroup equation (34) associated with equation (40) for the multiple atom target material of water. We consider the cases of discrete shield thickness $x_2, x_3, ...$ and apply the multigroup method to the solution of equation (16) applied to all target material $y > 0$. For each x_i-value considered, the initial conditions are obtained from the previous solutions generated where $y = 0$. This represents the application of the multigroup method to two different regions: region 1 of all shield material and region 2 of all target material. We then continue to apply the multigroup method to region 2 for each discrete value of shield thickness, where the initial conditions on the start of the second region represent exit conditions from the shield region 1. This provides for continuity of the solutions for the fluence between the two regions.

Reaction Effects on Evaporated Neutron Fields

In the present calculations, the two-stream bidirectional version of the multigroup method is always used because of its improved physical description and improved accuracy, especially near the boundaries of the incident radiation. Here, the assumption is made that half the evaporation source neutrons move in the forward direction and the other half move in the backward direction. The multigroup equations are, therefore, solved twice, once for the forward half of the source term and again for the backward half of the source. We evaluate the radiation fields for the solar particle event of February 23, 1956, in an aluminum slab 100 g/cm^2 deep with the results shown in figure 4 using the computational code of Heinbockel, Clowdsley, and Wilson (ref. 19) in which the evaporation neutrons are transported under elastic scattering only. Also shown in the figure are results obtained with the nonelastic process as described by the present calculation. A general decrease occurs in the 5 to 25 MeV neutron flux with a corresponding increase below 2 MeV. As one would expect, the more reactive energetic neutrons are removed from the field by the reactions with the appearance of lower energy neutrons as reaction products. Also shown are results from the MCNPX Monte Carlo code. It is clear that the discrepancies reported by Clowdsley (ref. 22) are not from neglect of nonelastic processes. Similar results are shown in figure 5 for a water target along with Monte Carlo calculations using the LAHET code (ref. 6). The discrepancies observed in our earlier calculations are clearly due to factors other than effects of reactive processes associated with the transport of evaporation neutrons.

High-Energy Backward Produced Neutrons

Although the two-body interactions of nucleons are limited to the forward scattering, the multiple scattering of nucleons in nuclei can produce a nucleon in the backward direction after several scattering events. In addition the Fermi motion within the nucleus will enhance this

effect. The angular distribution of nucleons from nuclear reactions was estimated by Ranft (ref. 23) to be given by the approximate function

$$g(A_t,E,\theta) = \left\{ \begin{array}{ll} N \exp\left(\frac{-\theta^2}{\lambda}\right) & (0 < \theta < \pi/2) \\ N \exp\left(\frac{-\pi^2}{4\lambda}\right) & (\text{Otherwise}) \end{array} \right\} \tag{74}$$

where $\lambda = (120 + 0.36A_T)/E$, with E the secondary particle energy in MeV, A_T the atomic weight of the struck nucleus, and N a normalization constant. The fraction of neutrons produced in the forward direction is

$$F_{\text{for}} = 2\pi \int_{\text{for}} g(A_T,E,\theta)\, d(\cos\theta) \tag{75}$$

The corresponding backward-produced neutron fraction is

$$F_{\text{bac}} = 1 - F_{\text{for}} \tag{76}$$

The approximate isotropic component of the interaction can be taken as

$$F_{\text{iso}} = 2F_{\text{bac}} \tag{77}$$

In earlier development of the multigroup method, we assumed that the direct reaction products would mainly be of high energy and in the forward direction and, therefore, adequately solved by the HZETRN code. The assumed isotropic evaporation source was then treated with the multigroup method by assuming half of the evaporation source was propagating in the forward direction and the second half in the backward direction. In similar fashion, we replace evaporation and direct reaction spectra in the code as follows:

$$\left. \begin{array}{l} f^e(E,E') \rightarrow F_{\text{iso}}[f^e(E,E') + f^d(E,E')] \\ f^d(E,E') \rightarrow F_{\text{HZETRN}}[f^e(E,E') + f^d(E,E')] \end{array} \right\} \tag{78}$$

where $F_{\text{HZETRN}} = 1 - F_{\text{iso}}$. These replacements (eqs. (78)) were made in the new version of HZETRN/multigroup code which is now only a minor modification. The terms on the right-hand side of equations (78) are shown in figure 6 and should be compared with figure 1. The importance of the reactive channels are accentuated because of the higher energies of the backward propagating neutrons.

Results for Ranft Modified Source

We have reevaluated the neutron fields in aluminum and water for the solar particle event of February 23, 1956, with the angular dependence of Ranft and the separations into HZETRN and isotropic components. The results are shown in figures 7 and 8 along with MCNPX (ref. 22) and LAHET (ref. 6) derived Monte Carlo results. The addition of the high-energy backward component is essential in reaching agreement with the MCNPX and LAHET codes. It is clear that the discrepancies observed by Shinn et al. (ref. 16) in the 50 to 200 MeV region are due to the energetic neutrons produced in the backward direction as reasonably described by the Ranft formula. The Ranft formula appears to overestimate the backward component for oxygen because agreement is improved for the omnidirectional flux at larger depths although forward and backward components may be somewhat incorrect. Quite satisfactory agreement is obtained at the largest depths. Still many of the cross sections in the HZETRN code are crude and a continued effort to improve them is expected to further enhance the calculated results.

Improved Cross Sections

A program of improved cross sections has been in progress for several years. Greatest attention has been given to fragment events for heavy ions which have been significantly improved (refs. 24 and 25). Recent years of research have resulted in improved absorption cross sections (ref. 26) and improved production cross sections for the present study using the LAHET code with results in table 2. The effects of these new cross sections are shown in figure 9.

Table 2. Number of Nucleons Produced in Nuclear Collisions With Aluminum Atoms

	Cascade Nucleons				Evaporation Nucleons			
Energy, MeV	$n \rightarrow p$	$n \rightarrow n$	$p \rightarrow n$	$p \rightarrow p$	$n \rightarrow p$	$n \rightarrow n$	$p \rightarrow n$	$p \rightarrow p$
25	0.13	0.26	0.09	0.24	0.38	1.13	0.43	0.96
200	0.73	1.26	0.80	1.18	0.75	1.22	0.90	1.11
400	0.91	1.58	0.99	1.49	0.87	1.29	1.04	1.13
1000	1.48	2.12	1.59	2.02	1.30	1.69	1.55	1.44
2000	1.97	2.58	2.11	2.45	1.44	1.83	1.70	1.58
3000	2.32	2.92	2.49	2.76	1.48	1.86	1.72	1.62

Concluding remarks

The methods described herein greatly improve the HZETRN computer code's neutron transport predictions. To summarize, a bidirectional multigroup solution of the straight-ahead Boltzmann equation for elastic and nonelastic transport of low-energy evaporation neutrons has been implemented. The resulting computer code was added to the existing HZETRN computer code which was developed at the Langley Research Center. With the new modified code, various simulations were conducted to test its accuracy. The Monte Carlo codes LAHET and MCNPX were used as benchmarks of accuracy. The modified code with and without the inclusion of nonelastic scattering processes for the evaporation neutrons is compared with these benchmarks. The neutron fluences are calculated at depths in aluminum of 1, 10, and 30 g/cm^2. These depths were selected because they represent typical values of shielding associated with the constantly changing space environment encountered by astronauts. The shield material of aluminum is typical because of weight considerations in space. The neutron fluences are calculated at depths of 1, 10, and 30 g/cm^2 in water. Water is used to model human tissue. Including nonelastic scattering processes in the calculation of the transport of low-energy evaporation neutrons slightly improves the prediction of neutron fluence at low energies, but the prediction of neutron fluence at slightly higher energies, around 10 MeV, is decreased by this change.

The HZETRN code underestimates the fluence of neutrons in the range of 5 to 200 MeV. In an effort to fix this problem, a formula by Ranft was used to estimate the number of isotropic neutrons at each energy. Using the bidirectional multigroup method to propagate all the isotropic neutrons greatly improved the neutron fluence predictions.

The addition of improved production cross sections to the code showed only modest improvement to the predicted neutron fluence. In the future, more accurate absorption cross sections will be added to the code, but this is expected to also have only a modest effect.

References

1. Wilson, John W.; Cucinotta, F. A.; Shinn, J. L.; Simonsen, L. C.; Dubey, R. R.; Jordan, W. R.; Jones, T. D.; Chang, C. K.; and Kim, M. Y.: Shielding From Solar Particle Event Exposures in Deep Space. *Rad. Meas.*, vol. 30, 1999, pp. 361–382.

2. Wilson, J. W.; Cucinotta, F. A.; and Simonsen, L. C.: Proton Target Fragmentation Effects in Space Exposures. *Adv. Space Res.*, To be Published.

3. Wilson, John W.; Nealy, John E.; Wood, James S.; Qualls, Garry D.; Atwell, William; Shinn, Judy L.; and Simonsen, Lisa C.: Variations in Astronaut Radiation Exposure Due to Anisotropic Shield Distribution. *Health Phys.*, vol. 69, no. 1, 1995, pp. 34–45.

4. Wilson, John W.; Badavi, Francis F.; Cucinotta, Francis A.; Shinn, Judy L.; Badhwar, Gautam D.; Silberberg, R.; Tsao, C. H.; Townsend, Lawrence W.; and Tripathi, Ram K.: *HZETRN: Description of Free-Space Ion and Nucleon Transport and Shielding Computer Program.* NASA TP-3495, 1995.

5. Alsmiller, R. G., Jr.; Irving, D. C.; Kinney, W. E.; and Moran, H. S.: The Validity of the Straightahead Approximation in Space Vehicle Shielding Studies. *Second Symposium on Protection Against Radiations in Space*, Arthur Reetz, Jr., ed., NASA SP-71, 1965, pp. 177–186.

6. Prael, R. E.; and Lichtenstein, Henry: *User Guide to LCS: The LAHET Code System.* LA-UR-89-3014, Los Alamos Nat. Lab., 1989.

7. Nealy, John E.; Qualls, Garry D.; and Simonsen, Lisa C.: Integrated Shield Design Methodology: Application to a Satellite Instrument. *Shielding Strategies for Human Space Exploration*, J. W. Wilson, J. Miller, A. Konradi, and F. A. Cucinotta, eds., NASA CP-3360, 1997, pp. 383–396.

8. Wilson, John W.; Cucinotta, F. A.; Shinn, J. L.; Simonsen, L. C.; and Badavi, F. F.: *Overview of HZETRN and BRNTRN Space Radiation Shielding Codes.* SPIE Paper No. 2811-08, 1996.

9. Wilson, John W.; and Khandelwal, G. S.: Proton Dose Approximation in Arbitrary Convex Geometry. *Nucl. Technol.*, vol. 23, no. 3, Sept. 1974, pp. 298–305.

10. Wilson, John W.; and Lamkin, Stanley L.: Perturbation Theory for Charged-Particle Transport in One Dimension. *Nucl. Sci. & Eng.*, vol. 57, no. 4, Aug. 1975, pp. 292–299.

11. Lamkin, Stanley Lee: A Theory for High-Energy Nucleon Transport in One Dimension. M.S. Thesis, Old Dominion Univ., Dec. 1974.

12. Letaw, John; Tsao, C. H.; and Silberberg, R.: Matrix Methods of Cosmic Ray Propagation. *Composition and Origin of Cosmic Rays*, Maurice M. Shapiro, ed., D. Reiel Publ. Co., 1983, pp. 337–342.

13. Wilson, John W.: *Analysis of the Theory of High-Energy Ion Transport.* NASA TN D-8381, 1977.

14. Wilson, John W.; and Badavi, F. F.: Methods of Galactic Heavy Ion Transport. *Radat. Res.*, vol. 108, 1986, pp. 231–237.

15. Wilson, John W.; Townsend, Lawrence W.; Nealy, John E.; Chun, Sang Y.; Hong, B. S.; Buck, Warren W.; Lamkin, S. L.; Ganapol, Barry D.; Khan, Ferdous; and Cucinotta, Francis A.: *BRYNTRN: A Baryon Transport Model.* NASA TP-2887, 1989.

16. Shinn, Judy L.; Wilson, John W.; Nealy, John E.; and Cucinotta, Francis A.: *Comparison of Dose Estimates Using the Buildup-Factor Method and a Baryon Transport Code (BRYNTRN) With Monte Carlo Results.* NASA TP-3021, 1990.

17. Lamkin, Stanley L.; Khandelwal, Govind S.; Shinn, Judy L.; and Wilson, John W.: Space Proton Transport in One Dimension. *Nucl. Sci. & Eng.*, vol. 116, no. 4, 1994, pp. 291–299.

18. Shinn, Judy L.; Wilson, John W.; Lone, M. A.; Wong, P. Y.; and Costen, Robert C.: *Preliminary Estimates of Nucleon Fluxes in a Water Target Exposed to Solar-Flare Protons: BRYNTRN Versus Monte Carlo Code.* NASA TM-4565, 1994.

19. Heinbockel, John H.; Clowdsley, Martha S.; and Wilson, John W.: *An Improved Neutron Transport Algorithm for Space Radiation.* NASA/TP-2000-209865, 2000.

20. Wilson, John W.; Townsend, Lawrence W.; Schimmerling, Walter S.; Khandelwal, Govind S.; Khan, Ferdous S.; Nealy, John E.; Cucinotta, Francis A.; Simonsen, Lisa C.; Shinn, Judy L.; and Norbury, John W.: *Transport Methods and Interactions for Space Radiations.* NASA RP-1257, 1991.

21. Haffner, James W.: *Radiation and Shielding in Space*. Academic Press, 1967.

22. Clowdsley, Martha Sue: A Numerical Solution of the Low Energy Neutron Boltzmann Equation. Ph.D. Thesis, Old Dominion Univ., May 1999.

23. Ranft, J.: Lecture 22: The FLUKA and KASPRO Hadronic Cascade Codes. *Computer Techniques in Radiation Transport and Dosimetry*, Walter R. Nelson and Theodore M. Jenkins, eds., Plenum Press, 1980, pp. 339–371.

24. Wilson, J. W.; Tripathi, R. K.; Cucinotta, F. A.; Shinn, J. L.; Badavi, F. F.; Chun, S. Y.; Norbury, J. W.; Zeitlin, C. J.; Heilbronn, L.; and Miller, J.: *NUCFRG2: An Evaluation of the Semiempirical Nuclear Fragmentation Database*. NASA TP-3533, 1995.

25. Cucinotta, F. A.: Cluster Abrasion of Large Fragments in Relativistic Heavy Ion Fragmentation. *Bull. Am. Phys. Soc.*, vol. 39, no. 5, 1994, p. 1401.

26. Tripathi, R. K.; Wilson, J. W.; and Cucinotta, F. A.: Accurate Universal Parameterization of Absorption Cross Sections: II—Neutron Absorption Cross Sections. *Nucl. Instrum. & Methods Phys. Res. B*, vol. 129, no. 1, 1997, pp. 11–15.

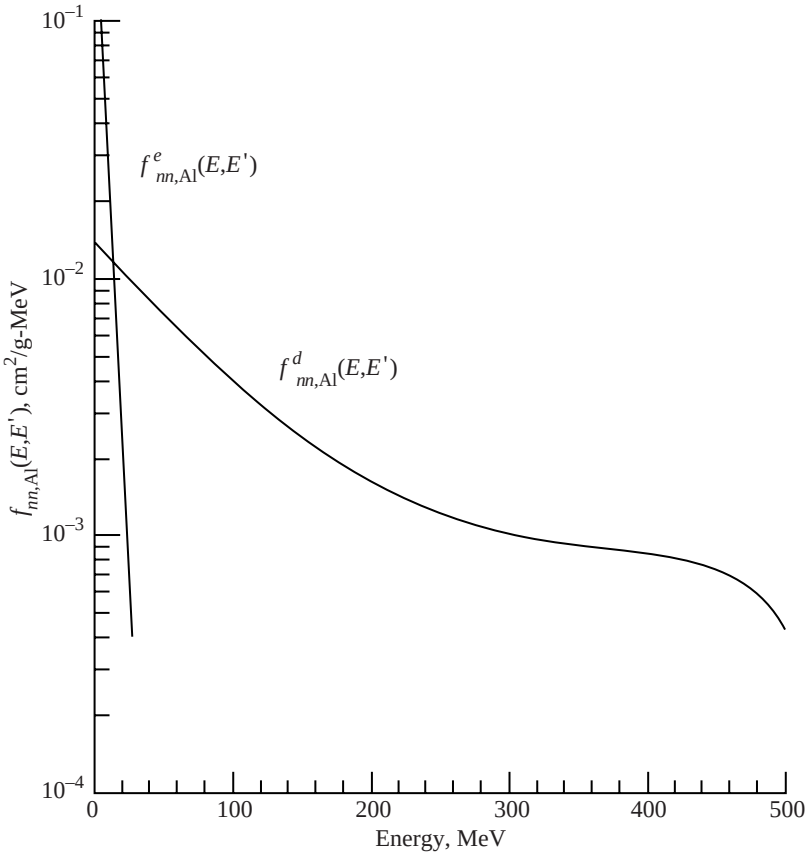

Figure 1. Evaporation and direct cascading neutron spectral effects for collision of 500 MeV neutrons in aluminum.

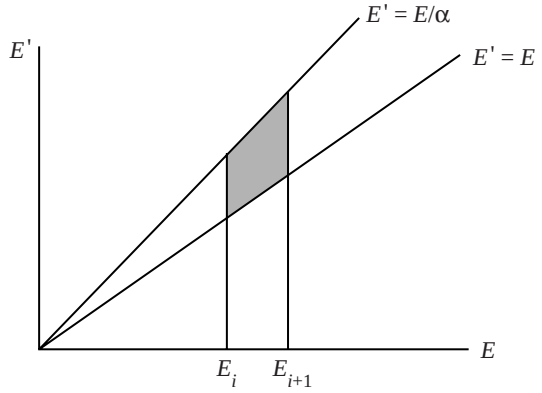

(a) General.

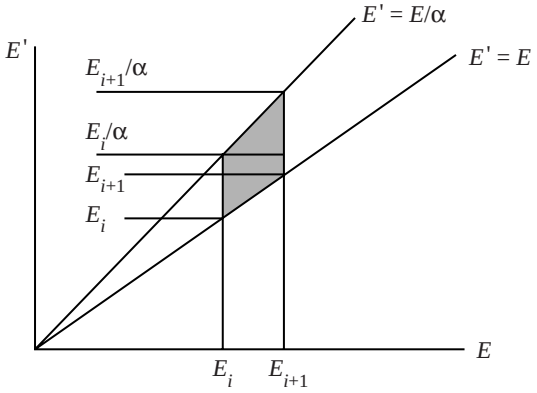

(b) $E_{i+1} < \frac{E_i}{\alpha}$.

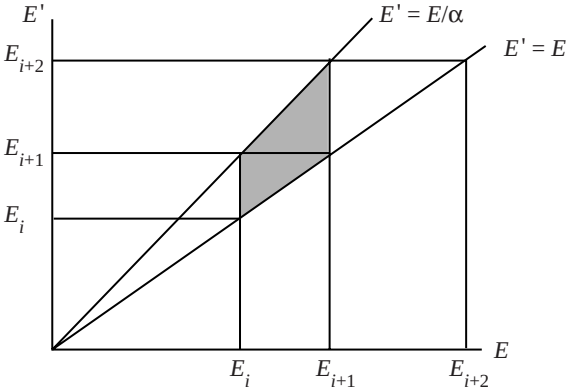

(c) $E_{i+1} = \frac{E_i}{\alpha}$.

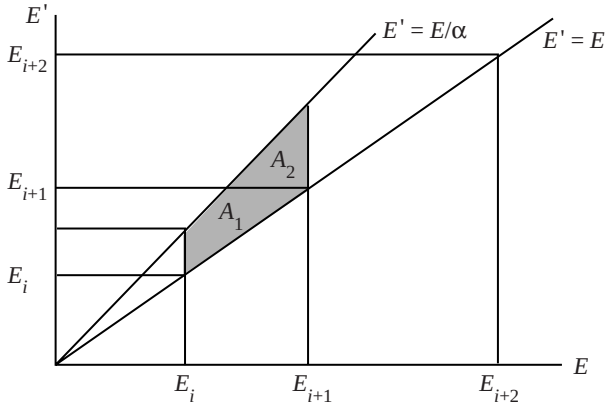

(d) $E_{i+1} > \frac{E_i}{\alpha}$.

Figure 2. Various energy partitioning schemes.

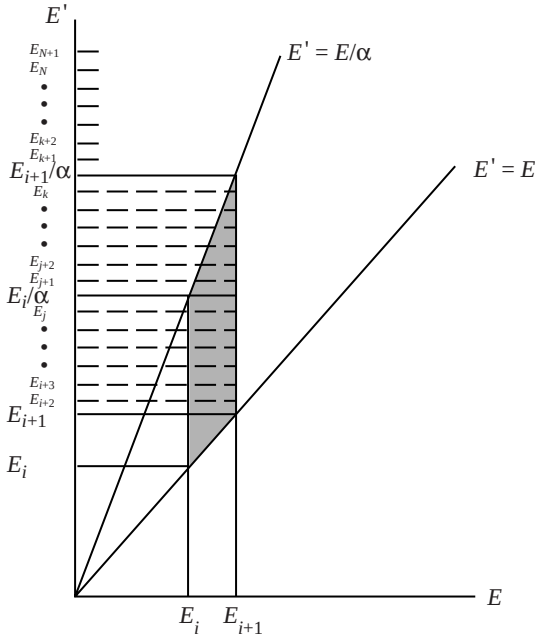

(a) $E_{i+1} < \frac{E_i}{\alpha}$.

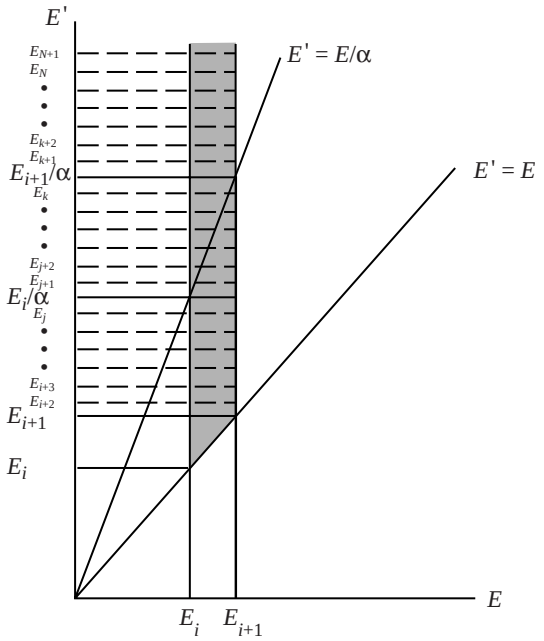

(b) Nonelastic scattering.

Figure 3. Multigroup energy partition.

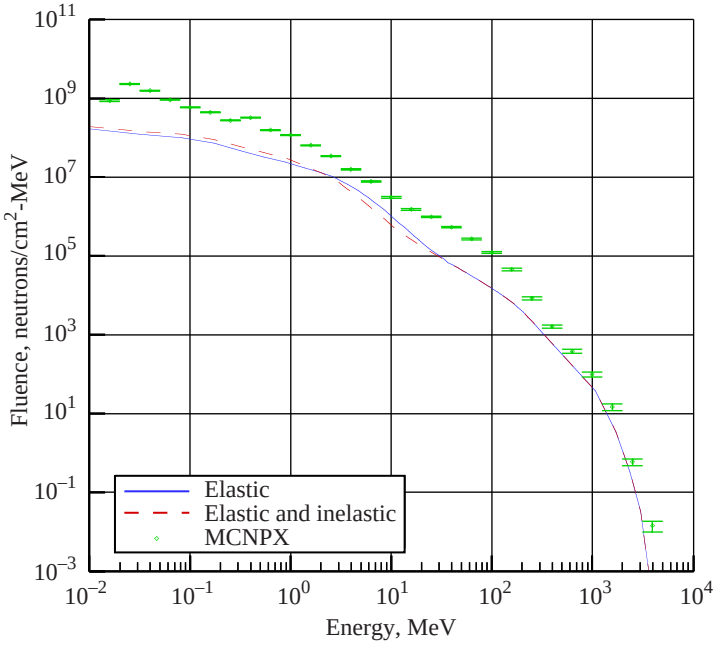

(a) Depth of 1 g/cm^2.

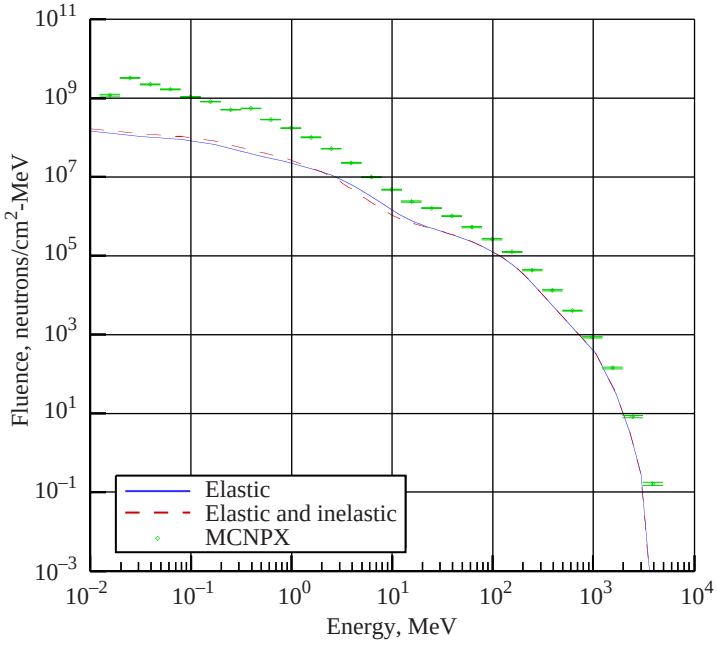

(b) Depth of 10 g/cm^2.

Figure 4. Energy spectra of neutron fluence in aluminum calculated by HZETRN program with bidirectional multigroup method used to transport evaporation neutrons.

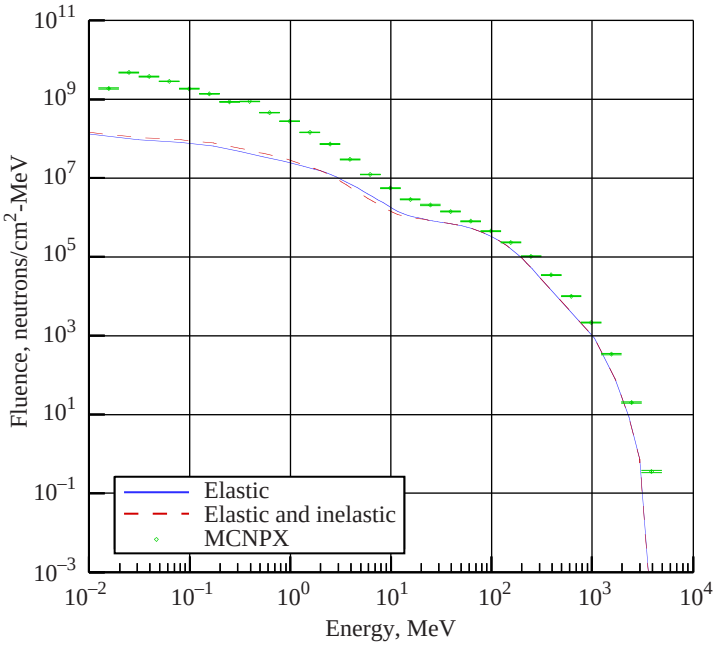

(c) Depth of 30 g/cm^2.

Figure 4. Concluded.

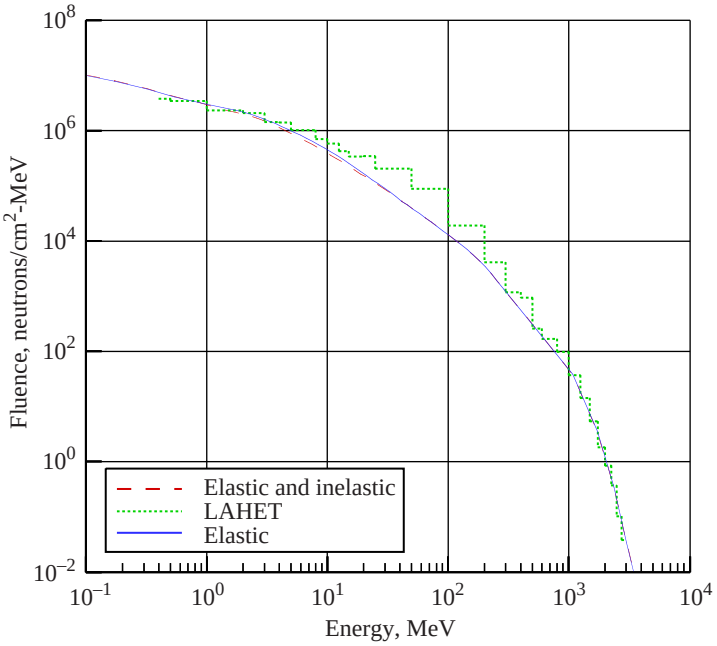

(a) Depth of 1 g/cm^2.

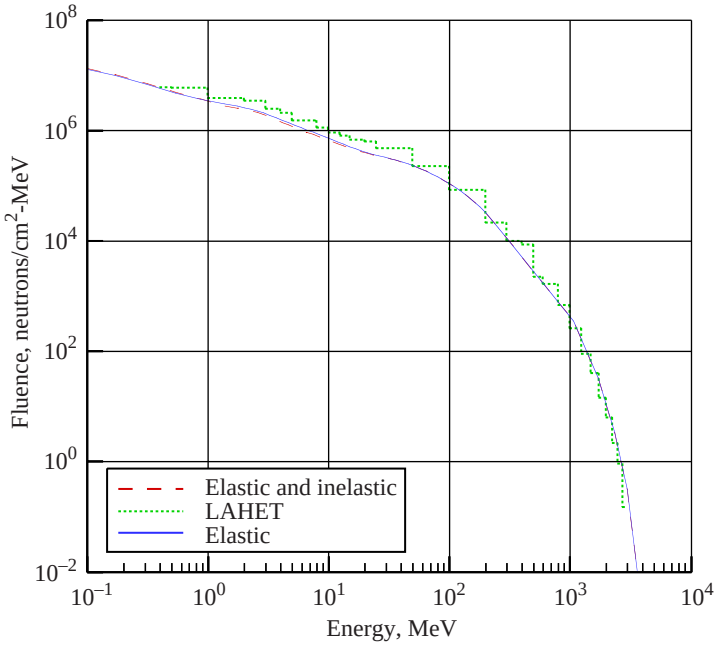

(b) Depth of 10 g/cm^2.

Figure 5. Energy spectra of neutron fluence in water calculated by HZETRN program with bidirectional multigroup method used to transport evaporation neutrons.

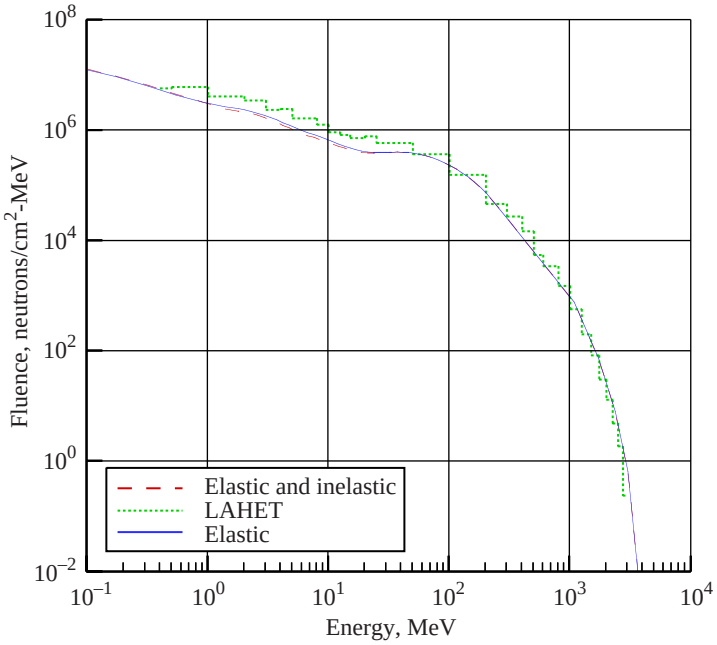

(c) Depth of 30 g/cm^2.

Figure 5. Concluded.

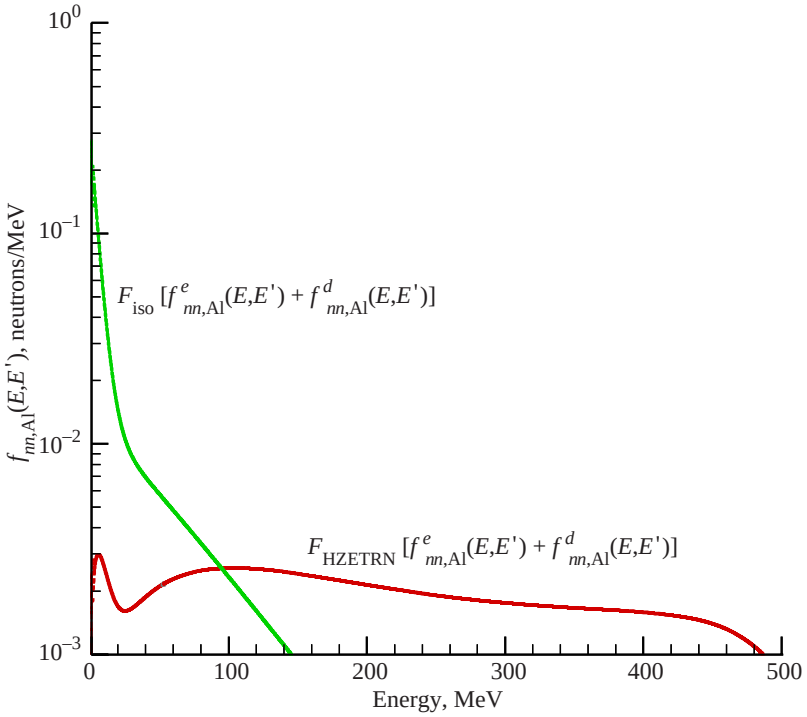

Figure 6. Forward moving and isotropic neutron spectral effects for collision of 500 MeV neutrons in aluminum.

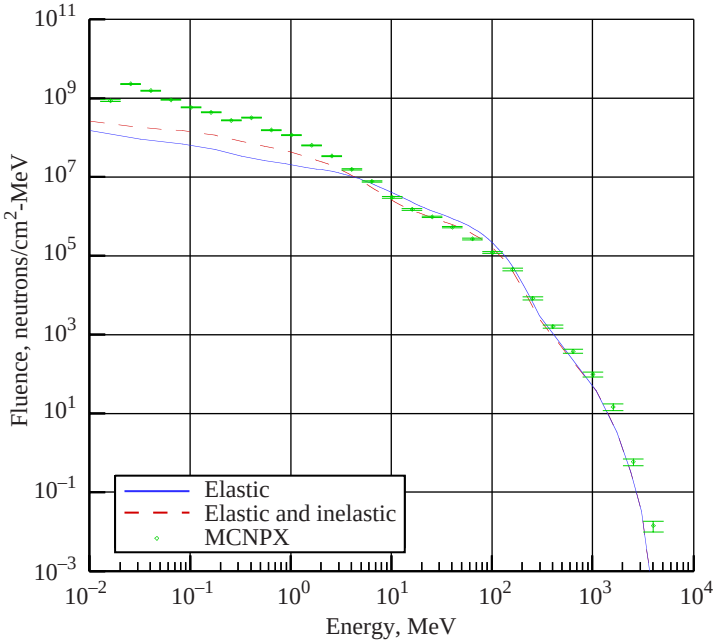

(a) Depth of 1 g/cm^2.

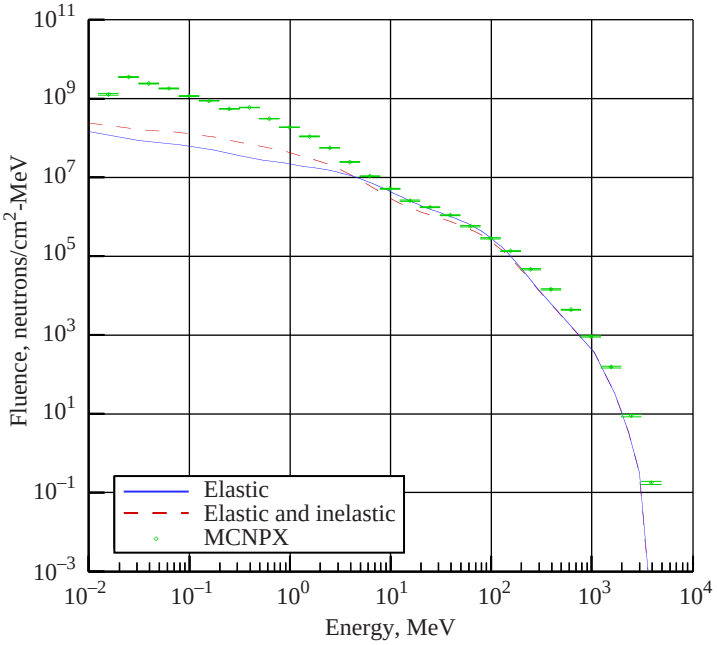

(b) Depth of 10 g/cm^2.

Figure 7. Energy spectra of neutron fluence in aluminum calculated by HZETRN program with bidirectional multigroup method used to transport all isotropic neutrons.

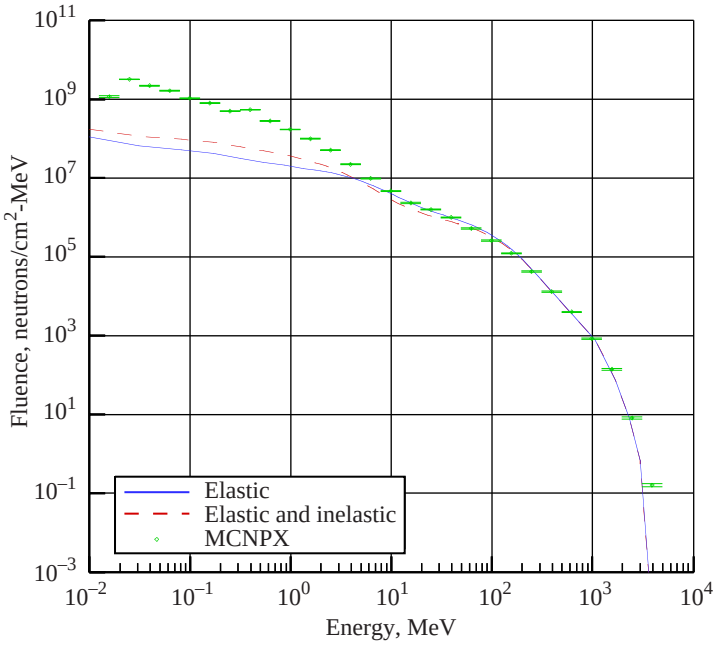

(c) Depth of 30 g/cm^2.

Figure 7. Concluded.

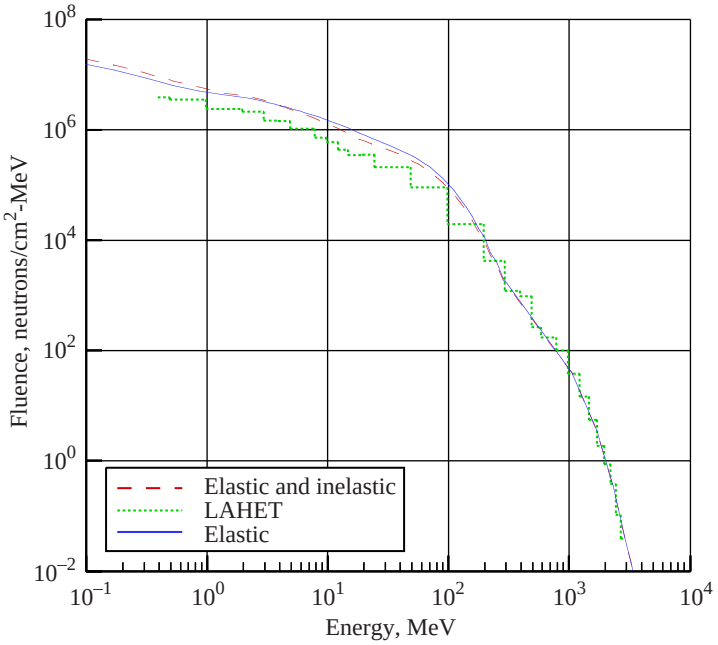

(a) Depth of 1 g/cm^2.

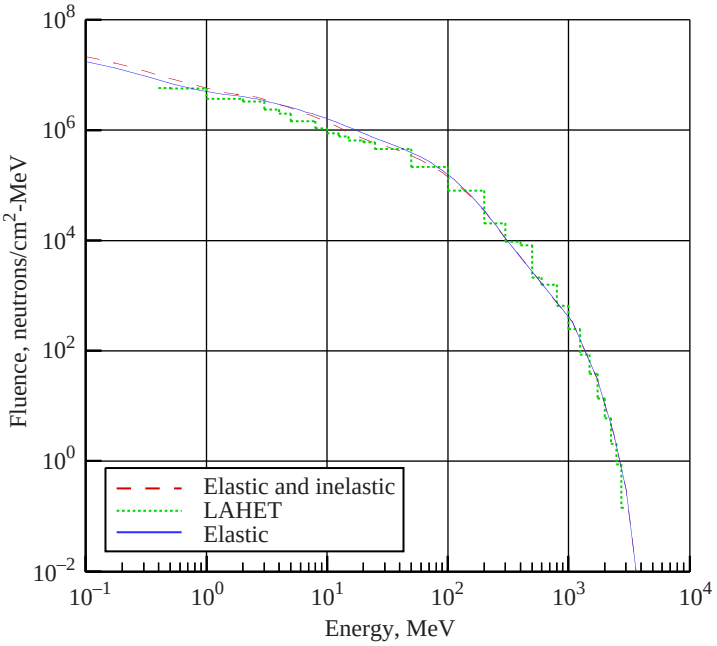

(b) Depth of 10 g/cm^2.

Figure 8. Energy spectra of neutron fluence in water calculated by HZETRN program with bidirectional multigroup method used to transport all isotropic neutrons.

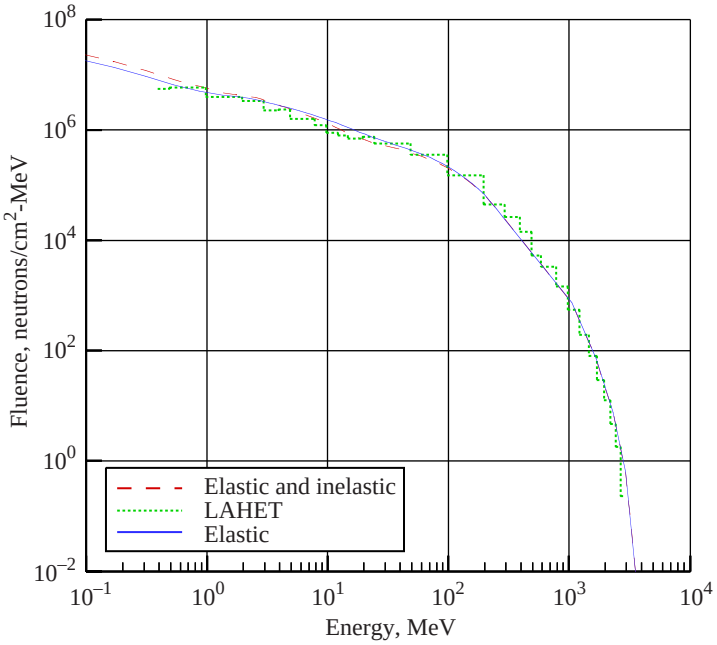

(c) Depth of 30 g/cm^2.

Figure 8. Concluded.

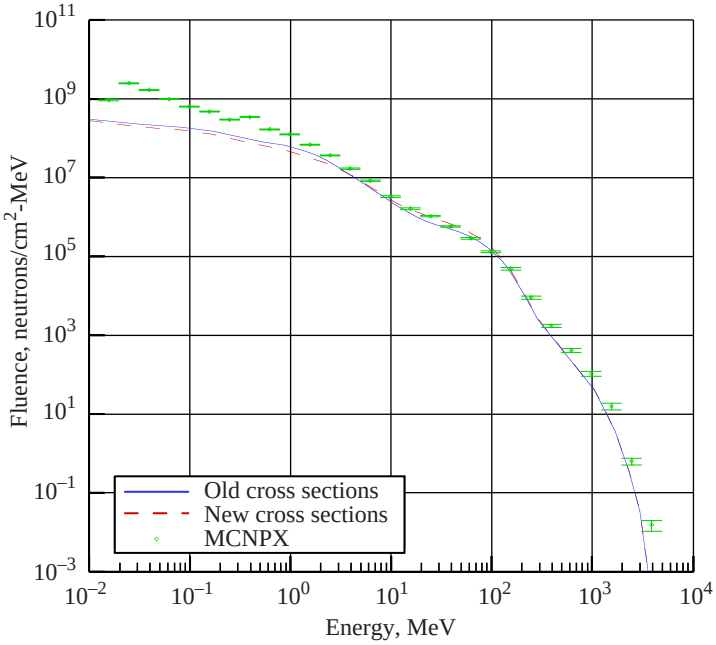

(a) Depth of 1 g/cm^2.

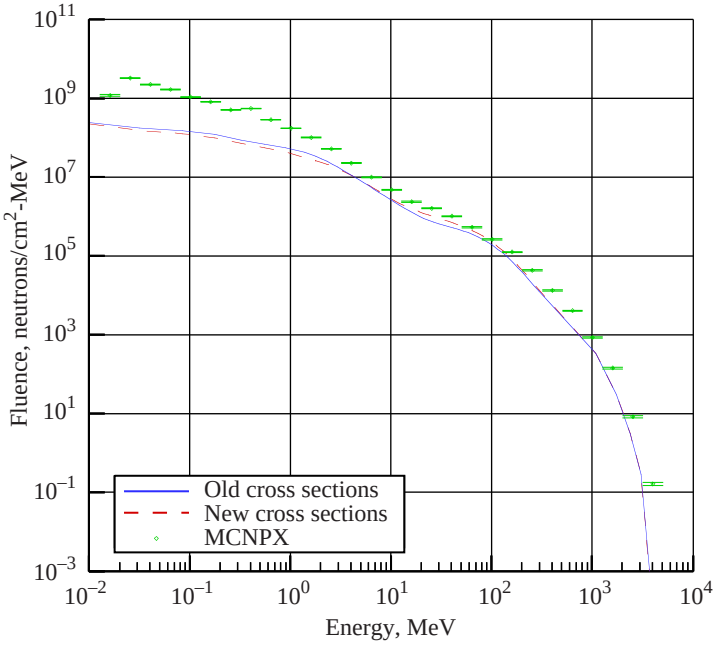

(b) Depth of 10 g/cm^2.

Figure 9. Energy spectra of neutron fluence in aluminum calculated with new cross sections.

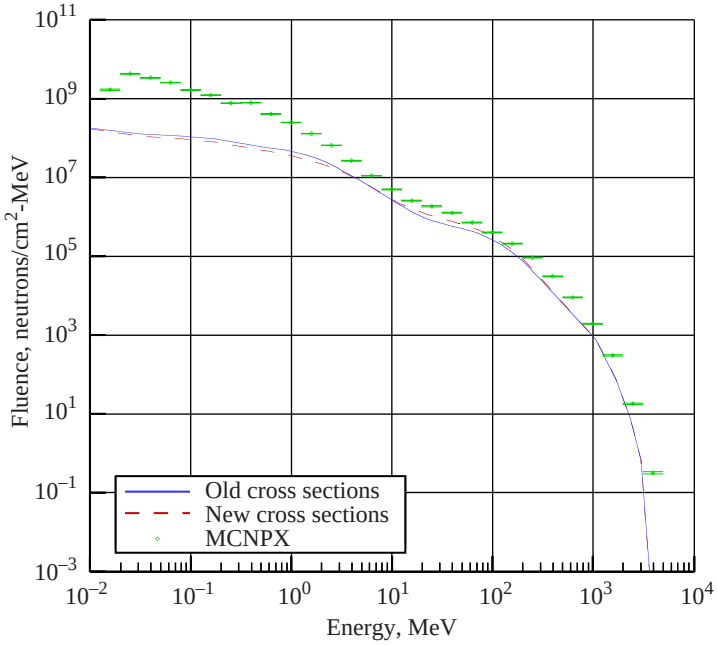

(c) Depth of 30 g/cm^2.

Figure 9. Concluded.

REPORT DOCUMENTATION PAGE

Form Approved
OMB No. 0704-0188

1. AGENCY USE ONLY *(Leave blank)*	2. REPORT DATE	3. REPORT TYPE AND DATES COVERED
	July 2000	Technical Publication

4. TITLE AND SUBTITLE
An Improved Elastic and Nonelastic Neutron Transport Algorithm for Space Radiation

5. FUNDING NUMBERS
WU 101-21-23-03

6. AUTHOR(S)
Martha S. Clowdsley, John W. Wilson, John H. Heinbockel, R. K. Tripathi, Robert C. Singleterry, Jr., and Judy L. Shinn

7. PERFORMING ORGANIZATION NAME(S) AND ADDRESS(ES)
NASA Langley Research Center
Hampton, VA 23681-2199

8. PERFORMING ORGANIZATION REPORT NUMBER
L-17971

9. SPONSORING/MONITORING AGENCY NAME(S) AND ADDRESS(ES)
National Aeronautics and Space Administration
Washington, DC 20546-0001

10. SPONSORING/MONITORING AGENCY REPORT NUMBER
NASA/TP-2000-210299

11. SUPPLEMENTARY NOTES
Clowdsley: NRC-NASA Resident Research Associate, Langley Research Center, Hampton, VA; Wilson, Tripathi, Singleterry, and Shinn: Langley Research Center, Hampton, VA; Heinbockel: Old Dominion University, Norfolk, VA.

12a. DISTRIBUTION/AVAILABILITY STATEMENT
Unclassified–Unlimited
Subject Category 93 Distribution: Standard
Availability: NASA CASI (301) 621-0390

12b. DISTRIBUTION CODE

13. ABSTRACT ***(Maximum 200 words)***
A neutron transport algorithm including both elastic and nonelastic particle interaction processes for use in space radiation protection for arbitrary shield material is developed. The algorithm is based upon a multiple energy grouping and analysis of the straight-ahead Boltzmann equation by using a mean value theorem for integrals. The algorithm is then coupled to the Langley HZETRN code through a bidirectional neutron evaporation source term. Evaluation of the neutron fluence generated by the solar particle event of February 23, 1956, for an aluminum-water shield-target configuration is then compared with MCNPX and LAHET Monte Carlo calculations for the same shield-target configuration. With the Monte Carlo calculation as a benchmark, the algorithm developed in this paper showed a great improvement in results over the unmodified HZETRN solution. In addition, a high-energy bidirectional neutron source based on a formula by Ranft showed even further improvement of the fluence results over previous results near the front of the water target where diffusion out the front surface is important. Effects of improved interaction cross sections are modest compared with the addition of the high-energy bidirectional source terms.

14. SUBJECT TERMS	15. NUMBER OF PAGES
Multigroup; Secondary neutrons; Neutron transport; HZETRN; Radiation shielding	40
	16. PRICE CODE: A03

17. SECURITY CLASSIFICATION OF REPORT	18. SECURITY CLASSIFICATION OF THIS PAGE	19. SECURITY CLASSIFICATION OF ABSTRACT	20. LIMITATION OF ABSTRACT
Unclassified	Unclassified	Unclassified	UL